Measurements and modeling of EMC, applied to cabling and wiring

Document Version:
Publisher's PDF, also known as Version of Record (includes final page, issue and volume numbers)

Please check the document version of this publication:

• A submitted manuscript is the version of the article upon submission and before peer-review. There can be important differences between the submitted version and the official published version of record. People interested in the research are advised to contact the author for the final version of the publication, or visit the DOI to the publisher's website.
• The final author version and the galley proof are versions of the publication after peer review.
• The final published version features the final layout of the paper including the volume, issue and page numbers.

Link to publication

Measurements and modeling of EMC applied to cabling and wiring

G. Bargboer

Measurements and modeling of EMC,
applied to cabling and wiring

PROEFSCHRIFT

ter verkrijging van de graad van doctor aan de
Technische Universiteit Eindhoven, op gezag van de
rector magnificus, prof.dr.ir. C.J. van Duijn, voor een
commissie aangewezen door het College voor
Promoties in het openbaar te verdedigen
op donderdag 12 mei 2011 om 16.00 uur

door

Geesje Bargboer

geboren te Hellendoorn

Dit proefschrift is goedgekeurd door de promotoren:

prof.dr.ir. J.H.Blom
en
prof.dr. W.L. Kling

Copromotor:
dr. A.P.J. van Deursen

To Marcel, Tobias and "the little one inside"

Samenstelling promotiecommissie:

Rector Magnificus,	Voorzitter, Technische Universiteit Eindhoven
prof. dr. ir. J.H. Blom,	Technische Universiteit Eindhoven, promotor
prof. dr. W.L. Kling,	Technische Universiteit Eindhoven, promotor
dr. A.P.J. van Deursen,	Technische Universiteit Eindhoven, co-promotor
prof. dr. F. Canavero,	Politecnico di Torino
prof. dr. P. Degauque,	Université des Sciences et Technologies de Lille
prof. dr. A.G. Tijhuis,	Technische Universiteit Eindhoven
dr.ir. J. van der Merwe,	Philips Innovation Services

Abstract

A myriad of cables transport power and communication signals in larger buildings and installations. Cross talk between cables and connected equipment is a major concern. Regulations do exist, but often show to be insufficient to avoid undesirable coupling. The present thesis research addresses this problem and provides a tested model for the interference coupling in buildings, in particular those caused by lightning. The model should also give an insight in the reliability of cabling and wiring, even when not all details of the installation are known. This was the goal as proposed in the IOP-EMVT project 'Optimal cabling in buildings and installations qua EMC'.

A newly built pharmaceutical plant acted as main test object. In the measurements, currents of 0.3 kA were injected in the lightning protection grid on the roof. Inside the building, 100 m long test cables followed the path of other installation cables on the ladders and trays. The measured current and voltage are typical for the other cables. A simplified model of the installation included most designed current paths. It was implemented in method-of-moments program FEKO. Measurements and model agreed that the roof steel skeleton carried about 80 % of the current and the intended lightning conductors 20 %. A nearby, non-intended conductor (an airduct) had to be included in the model to obtain acceptable agreement between the calculated current through a cable support and the measured one. For three types of cables, the measured voltages agreed with the currents when combined with the transfer impedance measured in the laboratory. The agreement allows extrapolating the model to real lightning. This has been done in two steps, the first and simple takes the cable transfer impedances into account; the second and more complicated also includes travel time and resonances in the installation. The differences between both are limited for the Profibus fieldbus cable and not for the 2-lead cable with steel armor. The transfer impedance of the cables showed the advantages of armored cables even inside buildings. Additional interconnects to ground constructions cause a reduction of the lightning current inside a structure. They reduce the excitation of internal building resonances and shift the resonance frequencies upwards. Unrealistic artifacts in model results should be avoided by including a sufficient number of interconnects.

Other shorter experiments are presented. For example: measurements and calculations on the lightning safety of an electronic lamp driver have been carried out on request of Philips Lighting. Based on the knowledge developed, an effective remedy

against unacceptably large damage could be given.

Simple configurations serve as direct test case for the models, such as the current distribution over a set of two 70 m long horizontal grounding electrodes. We compared measurements and the FEKO model, with simple analytical expressions. The interesting frequency range is up to 1 MHz, of relevance for lightning and conducted interference in switched mode power supplies.

Samenvatting

Een kluwen van kabels transporteert datasignalen en vermogens in gebouwen en installaties. Een belangrijk probleem is overspraak van signalen tussen kabels en daaraan verbonden apparaten. Er zijn normen, maar om de onwenselijke koppeling te vermijden zijn deze vaak niet afdoende. Dit onderzoek richt zich op dit probleem en voorziet in een beproefd model van storende koppelingen in gebouwen. In het bijzonder voor storingen veroorzaakt door bliksem. Het model zou inzicht moeten geven in de betrouwbaarheid van bekabeling ook al zijn niet alle details van de installatie bekend. Dit was het doel, zoals het was voorgesteld in het IOP-EMVT project 'Optimal cabling in buildings and installations qua EMC'.

Het belangrijkste test object was een recent opgeleverd gebouw van een farmaceutisch bedrijf. Tijdens de metingen zijn stromen van 0.3 kA geïnjecteerd in het bliksembeveiligingsdaknet. Binnenin het gebouw zijn 100 m lange testkabels aangebracht, die een route volgden die representatief is voor de andere installatiekabels in de daarvoor aanwezige kabelgoten en kabelladders. De gemeten stromen en spanningen zijn typerend voor alle kabels. Het meerendeel van de bewust aangebrachte strompaden in de installatie zijn gemodelleerd in een vereenvoudigd model. Dit model is geïmplementeerd in het method-of-moments programma Feko. Het is gebleken uit zowel de metingen als het model, dat de staalstructuur van het dak ongeveer 80 % van de stroom en de bliksemafleiders ongeveer 20 % van de stroom voerden. Om een acceptabele overeenkomst tussen de berekende en gemeten stromen in de kabelgoot te kijgen moest een onverwachte geleider in het model worden meegenomen. Namelijk, een ventilatieschacht, die dicht in de buurt van de kabelgoot lag. Voor drie typen kabels is er in het laboratorium naar de transferimpedantie gekeken. Uit deze metingen is gebleken dat de spanningen overeen met de gemeten stromen. Deze overeenkomsten zorgen ervoor dat het model kan worden geëxtrapoleerd naar echte bliksem. Dit is in twee stappen uitgevoerd, de eerste en meest simpele maakt gebruik van de transferimpedantie; de tweede complexere gebruikt ook nog de looptijd en de resonanties in de installatie. Het verschil tussen de twee is beperkt voor de Profibus fieldbus kabel, maar niet voor de 2draads kabel met stalen afscherming. De transferimpedantie van de kabels laat een voordeel voor het gebruik van gearmeerde kabels ook binnen in het gebouw zien. Extra verbindingen met de aardconstructie in de grond veroorzaken een vermindering van de bliksemstroom binnen in de structuur. Deze verminderen de excitatie van interne resonanties in het gebouw en verschuiven de resonatiefrequenties

naar hogere frequenties. Onrealistische verschijnselen in modellen kunnen vermeden worden door voldoende tussenverbindingen aan te brengen.

Verder zijn er andere kortere experimenten beschreven. Bij voorbeeld, metingen en berekeningen aan de bliksembeveiliging van een electronische lampballast zijn uitgevoerd op verzoek van Philips Lighting. Met de ontwikkelde kennis is een effectieve oplossing gevonden om een grote schade kan worden voorkomen.

Als voorbeelden voor de modellen zijn simpele configuraties gebruikt, zoals de stroomverdeling over een set van twee 70 m lange horizontale aardelectrodes. We hebben metingen en een Feko model met simpele analytische formules vergeleken. Het belangrijkste frequentiebereik loopt tot 1 MHz, dit bereik is relevant voor bliksem en voor geleidingsstoringen in geschakelde voedingen.

Contents

Chapter 1

Introduction

1.1 Electromagnetic Compatibility (EMC)

Almost all electronic equipment generates electromagnetic fields. These fields can disturb other systems through various coupling mechanisms. An electromagnetic interference (EMI) problem arises when three parts are present: a disturbance source, a victim and a coupling mechanism. When the problem is stated like this, three possible solutions are available. The problem can be solved, by modifying the disturbance source or modifying the victim to decrease the EMI. Most commonly the coupling mechanism is modified.

EMC means that a system fulfils these following three requirements:

1. it does not cause inconvenient interference to other systems (emission issues or causing EMI disturbance

2. it is not annoyingly susceptible to emissions from other systems (immunity systems) or susceptible for EMI disturbance

3. it does not cause self-pollution

The most common coupling path used between disturbance source and disturbance victim is the cable. A myriad of cables are used for transportation of power and communication signals. These cables can be unwanted antennas for the surrounding equipment, also. Most often there are regulations defined for equipment and its connections. However, surrounding equipment should also be taken into account. A lot of metal, air ducts and concrete reinforcements are present in the environment and can be used to conduct unwanted disturbances.

Since January 1st 1996, the European Economic Community (EEC) has imposed demands to equipment with respect to Electromagnetic (EM) disturbances. These demands do not include piping or movable equipment. All metal available in the environment can be used for protection of the signal and power cables. For this reason this construction, which has an electrical influence, should be taken into account during the design of a building. At the moment no models are present to support the designer of buildings.

Many EMC standards are developed in practice. There is often a lack in the theoretical EM basis. Part of the EMC work is laying a better basis for the measurement methods or developing better constructed measurement methods. The intensified usage of the electromagnetic spectrum should also be taken into account. For example: an office with one or two mobiles and a PC with Wifi; using a bluetooth connection with the mobile to synchronize appointments. As a result nowadays, much interest is shown for Reverberation Chambers [Nij09] and [Dij07]. These chambers mix EM fields to agree with these real-life environments. In these environments the EM fields are randomized and cause all kinds of disturbances in one measurement, like mentioned in the example. Generally EMC-tests are conducted at open area test-sites or in full-anechoic or semi-anechoic test rooms, which are very controlled environments. In these environments the situation is varied and therefore time consuming.

1.2   Current scope

My research is continuing the research at the Eindhoven and the Delft Universities of Technology of Van Houten [Hou90], Van Helvoort [Hel95a], Van Horck [Hor98] and Steenstra [Ste08a]. They contributed to the development of understanding the protection of electronic equipment and also contributed to robust knowledge about details of an installation; such as the extent of the protection from cable trays and conduits. The thesis of Van Houten laid the basis for a standard by the International Electrotechnical Commission (IEC): IEC 61000-5-2 [IEC97]. This was the first proposition to implement the knowledge. An example of an application is given in the thesis of Van Waes [Wae03]. He implemented this knowledge to a 50 Hz power grid in cooperation with Nuon, a Dutch utility company. At ONERA, the French aerospace laboratory, Parmantier developed an arithmetic model for cabling and wiring in airplanes. This model is also used in cars. In both cases the outer construction consists of a metal chassis, which simplifies the model. However, this knowledge is less applied in the construction of buildings.

1.3   Lightning

A natural source of EMI is a lightning discharge, which is a high-current electrical discharge.

From the 8th century before Christ till about 300 after Christ lightning and thunder were associated with gods. The ancient Greek god and ancient Roman god are the most known, namely Zeus and Jupiter. Also known are Donar and Thor from the Teutons and Northmans and Seth of the Egyptian. In Slavonian countries it is assigned to Perun. The Etruscan assigned it to Tinia. In the East in Taoism it is assigned to Lei Gong, god of thunder, and his wife Tien Mu, responsible for lightning, or mostly in China to dragons. In South America the Azteks assigned this to Tlaloc.

In African countries people are terrified of lightning. A lot of accidents happen due to lack of protection and also due to the very wide open areas. Remarkably enough the African people do not assign lightning to a god. An example of an accident is the news of soccer teams hit by lightning in 1998. People in this part of the world

immediately look for shelter in case of a thunderstorm, which results in totally empty streets.

Roman Catholics have a lot of patron saints to turn to prevent damage in case of thunderstorms. One of them is Agatha of Catania, who lived around 250 after Christ and died as a martyr. Another patron is Scholastica of Monte Cassino. She is the sister of the patron Benedictus and the founder of a nunnery.

Lightning is an electrical discharge, which was proved by Benjamin Franklin, more than 200 years ago [Uma94] and [Rak03]. Research on the physics of lightning started in the early 20th century. From 1920 till 1930 the classic model for the charge structure of a thundercloud was developed. In this model a negative charged region is found nearby a positive charged region and when lightning occurs the electric field changes. There are intracloud discharges, which occur internally in a cloud, cloud to cloud discharges, cloud to air discharges and the most studied are cloud to ground discharges. To create a cloud to ground lightning discharge a cloud and ground both should have a charged region. In case of a negative cloud to ground lightning, the cloud should be negatively charged and the ground positively. Then a stepped leader is formed from the cloud to the ground till the surface electric field, between the surface and the tip of the leader, exceeds the breakdown strength of air. In this case upward moving discharges of the surface are initiated. When the upward and downward discharge connect the first return stroke is established. Generally another stroke can come down the established path or use a part of the path, as shown in Fig. 1.1. These strokes are called subsequent strokes.

Nowadays, there is much interest in lightning phenomena. This is shown in several conferences or special sessions of conferences and special editions of IEEE Transac-
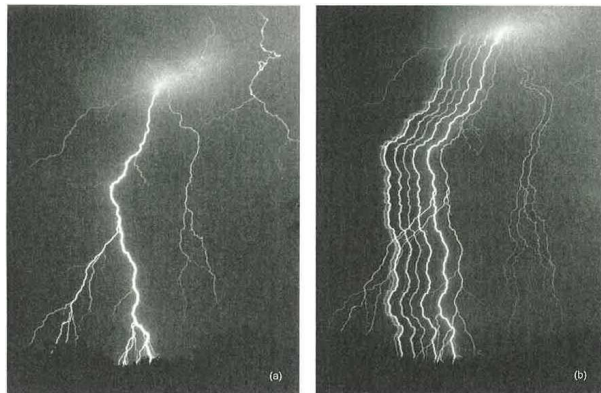
Figure 1.1: A lightning flash which appears to have at least seven (perhaps as many as ten) separate ground strike points; a) still camera photograph b)moving camera photograph. Some of the strike points are associated with separate branches of the same stroke while others are associated with the fact that different strokes take different paths to ground. The first and second strokes exhibit unconnected branches. The second and the third strokes, second and third from the right on the streaked photograph, are brighter than the first stroke, on the far end. Adopted from Fig. 4.1 [Rak03], who adopted it from Hendry (1993) [Hen93]

tions. Examples are the International Conference on Lightning Protection (ICLP), the Siposio International de Protecao Contra Descargas Atmosfericas (SIPDA), EMC Europe and the Asian-Pacific EMC (APEMC).

1.4 Goal of the research

This research is financed by the Dutch Ministry of Economic Affairs, Agriculture and Innovation and as such part of the Innovatief Onderzoeksprogramma Electromagnetische Vermogenstechniek, or IOP EMVT program [EMV11]. The EMVT can bring up solutions for all kind of problems in the field of energy. EMVT is a combination of technologies, which are applicable in integrated electromagnetic equipment with a high power density, high frequency and high efficiency, taking electrical, thermal and mechanical design facets into consideration. The immunity against electromagnetic influences and disturbances plays an important role.

The goal of the research is to define a model for the disturbance current in buildings, in particular caused by lightning.

Reliable interaction of equipment in buildings is essential to every modern installation. The EMC knowledge should already be implemented in the design phase of a building, because problem solving afterwards often results in high costs. The developed model should eventually, be implemented in the design of buildings.

1.5 Modeling

Models are generally used to define real-life applications. More and more computer models are used instead of real-life experiments to reduce costs. Simple models are verified with corresponding simple experiments. Then the models are extended to complicated situations to give insight in these situations. In this thesis the experiments are rather complicated and verified by simple models and also extended to a complicated situations again. The simple model in this thesis is used to extrapolate the measurements to real lightning currents and frequency. The original measurements could not be performed with lightning currents or a current of 1.5 kA, because it could pose a threat to systems according to the owners of the system, see Chapter 2. As a result the measurements are performed with smaller currents.

1.6 Thesis outline

Most of the chapters of this thesis have been published or submitted for publication. The reported simulations are performed with a commercially available computer code FEKO based on the Method of Moments [Fek10].

Chapter 2 deals with a newly built pharmaceutical plant, of which lightning protection has been investigated by measurements. A reduced model of the building incorporated most of the intended current paths. The measurements and model have been combined and extrapolated to actual lightning.

In Chapter 3 we extend the model of Chapter 2 and calculate the response of the installation on lightning currents, and include resonances in the cable trays and test cables contained in the trays.

In Chapter 4 two simplified models for a large building are compared for their lightning protection properties, one without and one with interconnecting conductive elements.

Chapter 5 reports the results of two short one-day current injection measurements on the lightning protection of two industrial buildings. This chapter gives insight in results from short measurements with too many unknowns to derive a model.

Chapter 6 describes measurements and calculations of a lightning test on an electronic lamp driver. This lamp driver with lightning protection is an example for an installation with cables and wires. Whether simple remedies could be found such as improved cabling in the posts or replacing all drivers was the question to answer. A simple remedy turned out to be very effective in the installation, namely the addition of a ground wire between armature and ground.

Chapter 7 covers measurements and a model to derive the current distribution over a set of two horizontal grounding electrodes for frequencies between 50 Hz and 1 MHz. Such systems can be used as grounding structures for lightning protection.

In Chapter 8 conclusions and recommendations for future work are presented.

Appendix A describes the implementation of a lightning channel by means of an antenna. Resistances are implemented in this antenna according to a Wu-King distribution. This method is used to eliminate the effect of resonances caused by the use of this antenna.

Appendix B shows the equations used to translate measured S-parameters into transfer parameters used to perform the calculations.

Appendix C shows the parameters for the lightning currents according to [IEC06], which are used in different chapters.

Chapter 2

A case study on lightning protection of a pharmaceutical building

A newly built pharmaceutical plant has been investigated by measurements. 100 m of test cables followed a path typical for cables belonging to the installation inside the building. Most of the designed current paths were incorporated in a reduced model of the building. We determined for three types of cables the transfer impedances. The measurements and model in this chapter have been combined and extrapolated to actual lightning. This work is published in an internal report and in short at different conferences in [Bar08], [Bar09], and in detail published in [Bar10]. The version in this chapter is adapted to the thesis.

2.1   Introduction

Lightning protection (LP) design is often based on rules derived from practical experience and sound reasoning [IEC06]. Periodic visual inspection of the LP system is recommended, with tests on the resistance to ground. For high risk buildings or structures and buildings with a large economical value it would be advisable to test the whole building with current injection, but such tests are not foreseen in [IEC06, Part 1, annex D]. A well known exception is the certification procedure for airplanes. The injection current should have a sufficient amplitude and sufficiently short rise time to resemble the real threat. These requirements are hard to meet for a large structure, such as a building. A work-around is possible when the major part of the protection relies on metallic conduction. In this case the protection behaves linearly unless arcing-over changes current paths. The tests can be performed with a current of lesser amplitude, and lightning induced currents and voltages can be obtained by extrapolation. Small currents also avoid damage to inadequately protected equipment during tests. Nevertheless, the injected current should have a sufficiently high frequency content to be representative for lightning. The current distribution in the building depends on the internal and external impedances of the conductors. The external impedances are inductive, and dominate the internal even taking the skin

effect of steel into account (see also Subsect. 2.4.1). As a result, the frequency is a common factor for all relevant impedances. The current distribution then does not strongly depend on frequency, until resonances show up. The measurement frequency of 18.4 kHz lies within this range for the building studied; the first resonance occurs at 0.9 MHz. The first quarter sinewave has a duration of 9 μs, which compares reasonably well with the rise time of the first stroke in [IEC06, Part 1, annex A].

LP is usually described in terms of routing of large currents, reduction of magnetic fields and induced voltages in large open loops [IEC06, Zis06, Ker07, Met06]. A complementary approach focusses on currents and reduction of the transfer impedance (Z_t). Inside the building all cables are supported by metal ladders and trays that form a continuous conducting structure integrated with the lightning protection. This way of interconnection has been advised before and implemented during construction. The support acts as "earthed parallel conductor" (EPC) [IEC97, Deu93, Deu89, Laa98] and protects the cables and electronic equipment. Many cables have protective earth (PE) leads, shields or armors as additional EPC. The voltages at equipment terminals are then related to the induced cable common-mode (CM) current via the Z_t. The Z_t varies largely between cables and is a function of frequency for each cable. The open-loop voltage does not appear at equipment terminals when the EPCs are connected to the local ground at both ends. But it would do so without EPC or with EPC disconnected at either end.

Whether the total industrial system is lightning safe depends also on the equipment connected to the cables. This is outside the scope of this research. The aim is to investigate to what extent a limited model of a complex building agrees with the measurements performed, what the benefits of armored and shielded cables are, and what a tentative extrapolation to lightning gives. Numerous papers appeared on the distribution of lightning currents in buildings with steel structures, e.g. [Ala02] and references therein. Often the structures studied are less complicated than actual industrial installations. Complicated structures are out of reach, but reduced models can provide useful predictions and insights.

2.2   Building and measurement set-up

The four floor building of 69 m (w) x 72 m (b) x 21 m (h) is a new plant for production of medicines. The measurements were requested after the building was constructed and most of the electrotechnical installation was completed. Fig. 2.1 shows the layout of relevant conductors on the roof and fourth floor with air treatment installations. To intercept the lightning current, a coarse grid of 50 mm^2 copper wire on the roof is assisted by a large number of 3 m tall rods [see Fig. 2.1(a)]. A steel skeleton gives the top floor its structural strength and supports the concrete roof plates [see Fig. 2.1(b)]. The grid is connected to the steel skeleton at many points on the edge of the roof, at a few points near the air-cooling units on the roof, and at mid-roof [dots and squares in Fig. 2.1(a)]. At the facades, the steel skeleton rests on reinforced concrete poles and is connected to downconductors leading to the foundation grounding. A buried ring around the building and rod electrodes placed at approximately 12 m spacing complete the outer LP. The total resistance to earth is smaller than 1 Ω. Inside the building, interconnected metal ladders and trays support the cables. The part on the fourth floor shown in Fig. 2.1(c) is typical for all other paths, only the horizontal
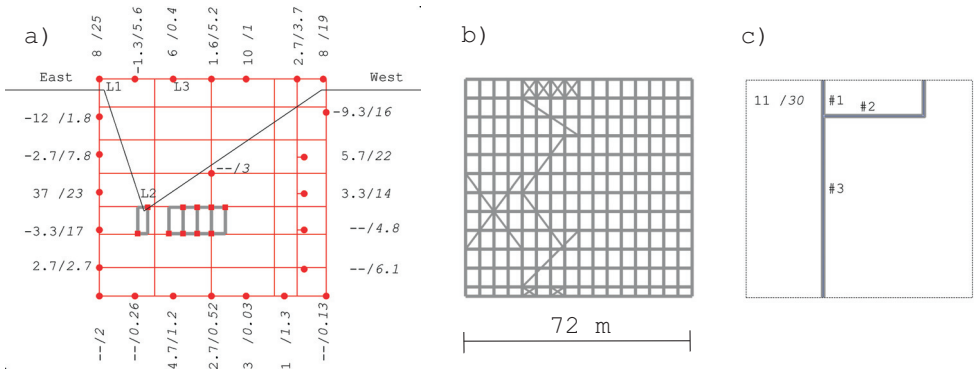
Figure 2.1: Three horizontal layers. (a) Roof grid at 19 m height with source position and HV leads indicated; the dots show the connections between roof grid and steel skeleton. Currents between grid and skeleton at the building edge and middle point are indicated (measured/*calculated*). (b) Top of the steel skeleton at 18.5 m height. (c) Cable support path at 16 m height. The lightning attachment positions L1, L2, and L3 in (a) and branches #1, #2, and #3 in (c) are discussed in Sections 2.2 and 2.5

extension is displayed. Two bundles of four 100 m long test cables have been laid for the measurements. The selection contained data and power cables, shielded, armored or unshielded, all of them samples of those used in the actual installation. One bundle ran over support branches #1 and #3, the other over #2 and #3. Near the facades, the cables followed a vertical path downwards over the distance of 2, 15, and 15 m at the ends of branch #1, #2 and #3, respectively.

The current source was placed on the roof, at the frame of a spare location for an
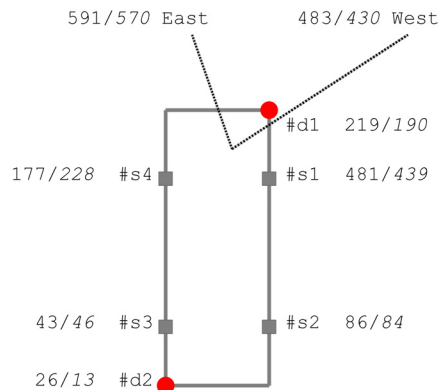
Figure 2.2: Current distribution on the frame carrying the source. (Dashes) HV leads. (Dots #d1-2) Connection of frame to roof grid. (Squares #s1-4) Conducting short pillars between frame and steel skeleton. The current values measured/*calculated* have been normalized to 1 kA at the source.

Figure 2.3: Photograph of connection of three cable ladders. The white ellipses emphasizes the two test cable bundles.

air-cooling machine. Four short steel pillars carried the frame and connected it to the skeleton. At opposite edges the frame was connected to the roof grid (see Fig. 2.2). A 0.5 μF, 40 kV capacitor was the current source; a spark gap acted as switch. The "cold side" of the source was connected to the frame. From the "hot side" long Filotex high-voltage (HV) leads ran at 2.5 m above the roof toward two grounding electrodes at 50 m distance from the building on opposite sides. The electrode resistances were 8.9 Ω (east) and 11.6 Ω (west) at the time of installation. The V-shaped path of the HV leads on the roof is indicated in Figs. 2.1(a) and 2.2. A 27-μH coil in series with the capacitor limited the current in case of an inadvertent short circuit.

To ensure linearity, the currents were measured with air-core Rogowski coils combined with active/passive integrators [Deu06]. Pearson current probes, with a conversion factor of 0.1 V/A, are used for smaller currents. For the voltage measurements, we used standard probes and battery-powered digital scopes. The bandwidth of the current measurements is minimally several hundred kH, sufficiently large to accurately record the transients.

Originally we planned to increase the injection current gradually from 100 A up to 1.5 kA, only to be limited by accidental mishaps in other electronic systems. One cable loop of the fire detection system was mounted against the top floor ceiling, just under the roof LP grid and skeleton. The owners of that system imposed a maximum voltage induced in their system to 35 V or a CM current of 1 A, which was met by limiting the injection current to 0.3 kA. The test cables shared the supports with power and signalling cables of other systems that were operating (see Fig. 2.3). The switched mode power supplies to which some of the other cables were connected generated quite some disturbances in the test cables. We improved the signal to noise ratio by averaging up to 100 records. This solution limited the number of measurements that could be performed in the available time. Experimental data in following sections will be scaled to the injection current of 1 kA.
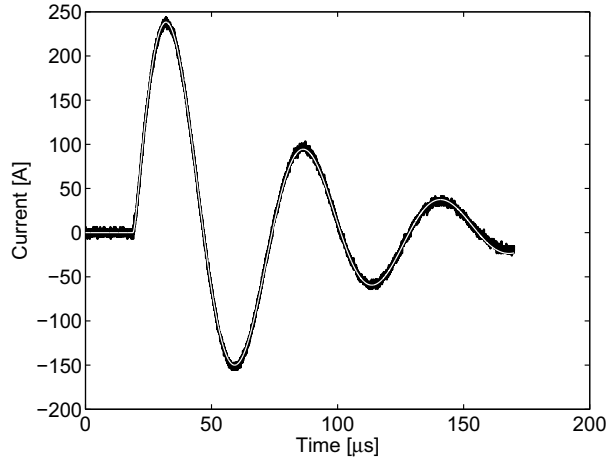
Figure 2.4: Example of the current injected in the LP at the pharmaceutical plant. The white line shows the fit to a single RCL circuit.

2.3 Measurement results

Fig. 2.4 shows an example of the injected current and the fit assuming an RCL circuit. Circuit parameters can be derived from the known capacitor value $C = 0.5\ \mu$F and the fit parameters: the resonance angular frequency is $\omega_d = 1.15 \times 10^5$ s^{-1} or frequency $f_d = 18.4$ kHz, the selfinductance $L = 150\ \mu$H and the resistance $R = 5.11\ \Omega$. The resistance can be fully attributed to the grounding electrodes, which leaves no resistance for the building. This confirms the statement (see Section 2.1) that induction determines the current distribution in the building. The peak current varied less than 10 percent over many discharge cycles.

Fig. 2.1(a) includes the peak currents through the connections between the LP grid and the steel frame at the building edge, normalized to a source current of 1 kA. The total measured current at the roof edge connections is 6% of the source current. As a general trend, the current returns near the source and under the HV leads (see

Table 2.1: Cables parameters: the three-lead unshielded power cable, the armored twin-lead power cable and the fieldbus cable. Current and voltage data in the first and last row have been measured with the T-shaped HV leads on the roof, the other two with the V-shape as in Fig. 2.2.

Type	R'_{dc} [Ω/km]	$|Z'_t|$ (18 kHz) [mΩ/m]	I_p [A]	V_p [V]	Conf.
a) 3-ld.	6.8	31.	0.19	0.68	T
b) arm. 2-ld	7.41	17.4	0.025	0.054	V
c) fieldbus	9.5	12.	0.031	0.025	V
c) ,,			0.32	0.28	T

also [Zis06]). The phase reversals found at several connections are remarkable and may indicate that isolated loops are present under the roof.

Fig. 2.2 presents the currents leaving the frame under the source towards the skeleton (#sn) and towards the roof grid (#dn), and the currents through both HV leads. One observes that about 80 % of the current flows towards the skeleton that acts as a bypass for the grid. The remaining 14% leaves the grid at other connections with the skeleton such as at the other frames, the thick lines in Fig. 2.1(a).

The current through the cable support was measured at only one position, with a T-shaped layout of the HV leads directly on the roof instead of the V-shape as in Fig. 2.1(a). The value of 11 A/kA injection is also indicated in Fig. 2.1(c).

At the far end of the 100 m test cables, all PE leads and shields were short circuited to the cable support. Here "far" means as viewed from the measuring equipment. At the near end, the cable shield and/or PE lead were again connected to the support. The loop formed by the PE and the support can be considered as the CM current loop. At the near end, we measured the CM current and also the voltage induced between all other leads bundled together and the PE. If one considers the bundled leads as a single one, the voltage can be viewed as differential mode (DM) with respect to the PE or shield. The DM voltage and CM current relate via a transfer impedance Z_t. Peak values of the 18.4 kHz component in CM current and DM voltage are summarized in Table 2.1, normalized to 1 kA source current.
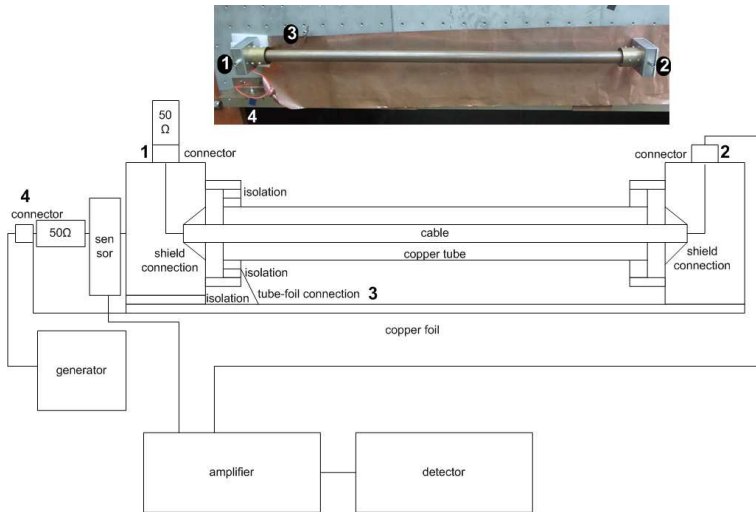
Figure 2.5: The transfer impedance Z_t measurement set-up for the very low frequency range. (Top) Picture of the measurement set-up. (Bottom) Schematic overview. Indicated are the connections to the generator, the sensor, the metal cases, the copper tube, the connectors, the resistances, the amplifier and the voltage meter. The cable is shown as wel as two connections. One connection indicates the inner conductors with the connector pins on top of the metal casings and the other indicates the inner conductor used as PE and the copper litz and armor connection with the metal casings. The numbers in the picture correspond with the numbers in the schematic overview.

2.3.1   Measuring cable transfer impedance

To retrieve the transmission line characteristic of the cable, measurements are performed with a triaxial measurement set-up as in [Ste08b]. Again, here the loop formed by the PE and the support is considered as the CM current loop and the DM voltage is considered between the leads and the PE or shield.

The three cables selected as exsamples are as follows:

a: a 3×2.5 mm^2 power cable with one PE lead;

b: a twin lead 2×2.5 mm^2 cable with steel armor and a 2.5 mm^2 copper litz as PE lead embedded in it; the armor has eight bundles of two wires of 0.3 mm diameter wound clockwise and eight bundles of eight wires in the opposite direction;

c: a 'Profibus' fieldbus [Pro10] cable for data transport with two 0.7 mm diameter copper leads inside a shield composed of an aluminum foil and spacious copper braid consisting of 16 bundles of five 0.15 mm diameter copper wires.

1 m segments of the test cables are positioned in a copper tube as indicated in Fig. 2.5. The inner leads are bundled together and are connected at both sides to the pins of the connectors on top of the metal casings. The connector pin on top of the metal casing at the left hand side is connected via a 50 Ω resistor to the metal casing. The connector on top of the metal casing at the right hand side is connected via the amplifier to the voltage meter. The inner conductor used as PE, if present, is connected with the copper litz, the shield and armor to the metal casings at both sides. The generator is connected via 50 Ω with the metal casing at the left hand side.

For measurements in the frequency range of 10 Hz to 1 MHz, the sine wave generator is the GW GFG 8050. This source has a current limitation of 400 mA. In other cases the generator is the Agilent 3320 A. The CM current sensor is a Pearson 110 current sensor. The voltage meter used was a EG&G model 5302 Lock-in. This detector measures both the amplitude and the phase. The voltage signals of the current sensor and the connector on top of the metal casing are connected to the amplifier EG&G mode 5113, to assure the measurement and the measurement-equipment loops were electrically separated. We amplify either 1 or 10 times.

Fig. 2.6 shows the measurement results for three cables.

For cable a one has

$$Z'_t = R'_{dc} + j\omega M', \tag{2.1}$$

with $R'_{dc} = 6.8$ mΩ/m the resistance of the PE lead, ω the angular frequency and $M' = 0.27$ μH/m the mutual inductance. The dashed line interpolates between the measured dc value and the high frequency Z'_t. The cross over frequency $R'_{dc}/2\pi M'$ is 4 kHz.

The construction of cables b and c is displayed in Fig. 2.7. Because of the armor or braid and foil outermost conductor, their $|Z'_t|$ rises much slower than cable a above 10 kHz. The $|Z'_t|$ of cable b rises proportional to $\omega^{0.4}$ (dashed line) between 5 and 500 kHz; the phase angle is about $\pi/6$. Above 1 MHz $|Z'_t|$ tends to rise $\propto \omega^{0.5}$ and the phase approaches $\pi/4$, appropriate for a Z'_t dominated by the skin effect. The fieldbus $|Z'_t|$ is nearly flat up to 2 MHz and increases proportional to $\sqrt{\omega}$ at higher
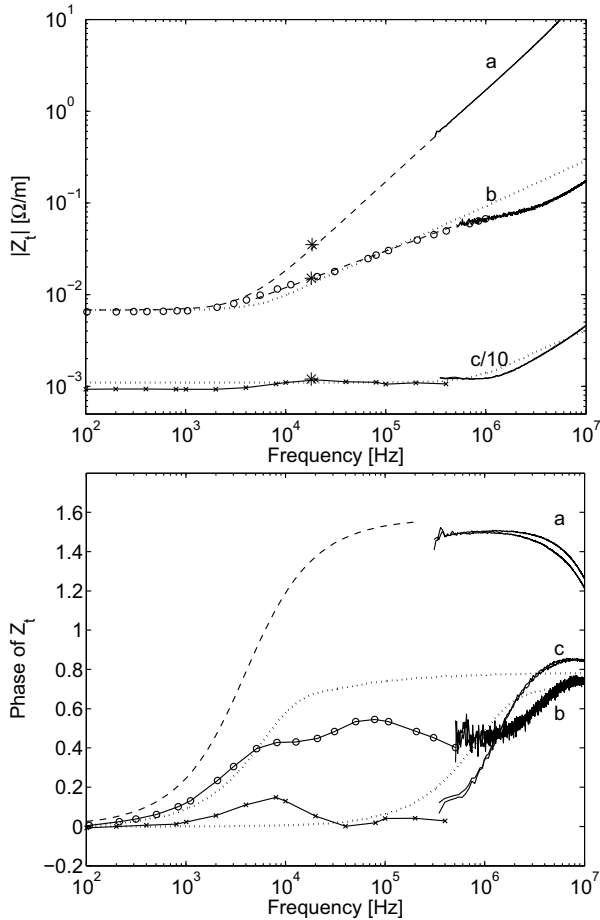
Figure 2.6: Measured and approximated transferimpedance of the three lead power cable a, the armored two lead power cable b and the fieldbus c in amplitude (top) and phase (bottom). The dotted lines are the approximations used for the extrapolation (see section 2.5). The markers $*$ show the $|Z'_t|$ values for the 100 m test cables.

frequencies whereas the phase tends to $\pi/4$. This behavior is analogous to the skin effect surface impedance, but it is rather unexpected for a cable with a foil shield. The small change in amplitude and phase near 10 kHz is tentatively attributed to the magnetic field penetration of the aluminum shield caused by the slit; a detailed investigation is outside the scope here. The ratio of measured peak current (I_p) and voltage (V_p) on the 100 m test cables in the building agrees with the respective cable Z'_ts at the injection frequency, as indicated by the markers in Fig. 2.6.
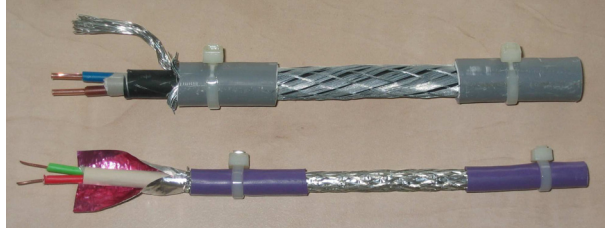
Figure 2.7: Samples of (top) the armored twin lead power cable and (bottom) the shielded Profibus cable.

2.4 Modeling

In order to reduce the complexity of the model, a limited number of conductors was taken into account, selected for their intended or probable contribution to LP.

2.4.1 Overall structure

The model starts with the conductors shown in Fig. 2.1 implemented in the commercial method of moments code [Fek08] (see also [Fek10]). The 50 mm^2 copper LP grid on the roof at 19 m height consists of meshes of approximately 20 m by 10 m. In Fig. 2.1(a), the grid and frames of the air-conditioning units are shown. Figure 2.1(b) shows the horizontal part of the steel skeleton at 0.5 m below the roof grid. The skeleton consists of I-beams (thick lines) modeled as 20 cm diameter tubes and of diagonal flat girders (thin lines) modeled as 10 cm diameter tubes. Vertical tubes of 20 cm diameter were included along the skeleton edge and extended downward. The layout of the cable support is shown in Fig. 2.1(c). As the model for the cable ladder, we choose two tubes of 7.4 cm diameter and one middle beam of 6.4 cm diameter 2.5 m below the roof grid; the cables were not included in the overall model. The vertical part of the paths is not shown in the figures. Fig. 2.2 shows the frame carrying the source in more detail. The dotted lines indicate the HV leads (diameter of 1.5 mm) in the V-shape configuration. A single 18 kHz voltage source is assumed between the HV leads junction and the frame. At the ends of the HV leads, the actual resistors (see Sect. 2.2) have been assumed. At four points (squares) the frame rests on the steel skeleton via short-conducting pillars. In view of the actual low resistance to ground (see Sect. 2.2), the soil under the building is regarded as a perfect conductor. A large amount of other metal present is neglected in this first model. All MoM segments have a maximum length of 4.5 m, and the total number of segments is about 5000. We tentatively introduced skin effect assuming a resistivity $\rho = 10\mu\Omega$·cm of steel, relative permeability of $\mu_r = 200$, and skin depth $\delta \approx 0.1$ mm. The currents varied less than 1% compared to the perfect conductor case. We did not consider skin effect further. These where negligible compared to other approximations.

The calculated impedance seen by the 18 kHz, 1 kA source is $5.04 + j11.25$ V/A. The imaginary part is equivalent to an inductance of 97 μH. If the 27 μH of the series coil is added, the total inductance is in reasonable agreement with the 150 μH from the fit on the measured current (see Sect. 2.3). The distribution of current over both HV leads agrees well with the measurements, as indicated in Fig. 2.2. It should

be noted that the HV lead currents have been measured separately from the source current, and minor variations occurred between discharges. The same good agreement holds for the distribution of current over the frame connections with the grid and the steel skeleton: the skeleton carries 80% of the current. Several connections between grid and steel skeleton were distributed over the roof, but these were not included in the model. As a result, the calculated sum of the currents towards the skeleton at the roof edge is 183 A, much larger than the 60 A measured. No phase reversals were found in the model.

The cable support current at #1 in Fig. 2.1(c) is 30 A in the model with the T-shape for the HV leads. This is nearly a factor of three larger than measured. A 0.8-m-diameter air duct ran close above the cable support. The duct was not an intended conductor because of rubber gaskets between the elements. However, the many bolts and metallic suspensions to the building structure made it a probable continuous conductor. When included in the model over the length of section #1 and #3 in Fig. 2.1(c), the duct reduced the support current to 17 A. With this result we decided not to include more conductors in the model.

The reinforced concrete roof plates were omitted in the model. The grids of different plates were physically separated and insulated. Such grids have only a local effect, and therefore do not contribute to the overall protection.

We verified that the current distribution remained the same when the frequency was increased from 18 to 180 kHz. This was to be expected, because induction determined the current distribution rather than the resistance at the grounding electrodes. We verified that the current 20%-80% distribution between roof grid and skeleton did not depend on the HV leads. A web-like structure of 12 HV leads evenly distributed over the building showed the same ratio. Actually, we would have preferred such an injection circuit for the measurements. The effect of a solid conducting floor has been studied in [Miy08]. We also included a metallic layer on the fourth floor; it left the current distribution above it nearly unchanged. However, equipment at floors below will see some benefit from it.

2.4.2   Cable support details

The cable ladders have rungs with 0.2 m separation. Many other cables share the support with the test cable bundle, but first we consider the latter only. The actual cross section of the ladder beams is shown in Fig. 2.8. The diameters in the overall model have been chosen to give an identical current distribution. The four test cables are taken as a bundle of 2 cm diameter, short circuited to the support at both ends. A 2-D static MoM code [Deu01b] resulted in the current distribution by requiring zero magnetic flux between the conductors. Rungs in the ladders short circuit the beams and reduce the magnetic flux through the openings. Because of the zero flux requirement in the MoM, one may omit the rungs. The part of the current through the test cable bundle is shown in Fig. 2.8 as a function of the bundle position over the dashed line. Many other cables share the support. We included four bundles of such cables in the same model while the test bundle was placed close to the middle beam, the position shown in Figs. 2.3 and 2.8. The current part through the test cable bundle decreased by a factor of 3. The measured ratio was 10% at branch #1 in Fig. 2.1(c). The model underestimated the cable bundle current. Again here, there
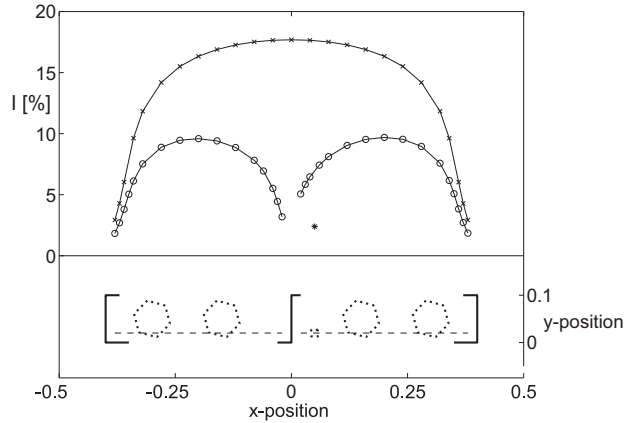
Figure 2.8: (Top)Test cable bundle current as a function of the position of the bundle, as percentage of the total current through the cable bundle and support, with (o) and without (x) the middle beam present. The marker * shows the value and position with four other bundles added (see section 2.4.2). (Bottom) Ladder beams (heavy lines) and assumed positions of cable bundle (dashes) for the top part. The dotted lines indicate the four other bundles.

remain many unknowns: variations in support (trays and ladders), in position and presence of other cables and their unknown terminations and possible pigtails.

2.4.3 Lightning simulation

A 200-m-tall vertical current path is assumed as model for the lightning channel. An 18 kHz voltage source with high internal impedance is positioned at half-height. The lower path connects the source and the building, the upper path is a free-standing antenna on top of the source. The current in upper path closes via the displacement current; most of the displacement current flows toward the soil. Three positions were chosen as attachment points to the building [see Fig. 2.1(a)]; L1 is at the corner of the building, L2 at the measurements injection point, and L3 on the roof edge exactly above the end of the branch #1 of the cable support. For the L1 position, the displacement current part on the building was determined as the difference between the current arriving at the corner and the sum of the conduction currents leaving via the connections to ground. The displacement current amounted to 3% of the injected current. In case of attachment at L2 the skeleton/grid current ratio remained 80% to 20%, and similar values in case of L1 and L3. The currents in the three support branches (#1, #2, and #3) are given in Table 2.2. The horizontal air duct has only small effect compared to the case of current injection with the HV leads.

2.5 Scaling to lightning

Under the assumption that the current distribution does not change, the model can be scaled up to the lightning parameters given in [IEC06, Part 1, Annex B]. These

Table 2.2: Calculated current in ampère through the cable support for a lightning current of 1 kA attached at points L1, L2 and L3 [see Fig. 2.1(a)]. The data are presented without/with air duct.

Position	#1	#2	#3
L1: Corner	10.1 / 7.8	6.1 / 5.2	3.9 / 2.5
L2: Inj. source	1.3 / 2.1	4.0 / 3.7	2.8 / 2.0
L3: Cable support	31.2 / 26	17.3 / 16	13.8 / 9.6

parameters can also be found in Appendix C. The transfer impedances of the test cables translate the currents into voltages that would be shared by equipment at both ends of the cables. Conservative values are obtained by taking the highest cable support current (#1 and L1 without air duct in Table 2.2) and the measured 10% for the cable bundle (Sect. 2.4.2). The finite-wave velocity over the supports and cables, and possible resonances have not been taken into account. Such effects could in principle be handled as detailed in [Bau78] and [Djo87]. Measurements showed that the bundle current is divided in a 3:3:2:2 ratio between two power cables and two thinner signal cables. A 200 kA lightning current pulse with 10 μs rise time, corresponds to severity level I (Table 2.3) for the first return stroke. The approximating expression for the lightning current i reads [IEC06]

$$i(t) = \frac{I}{k} \times \frac{(t/\tau_1)^{10}}{1 + (t/\tau_1)^{10}} \exp(-t/\tau_2). \qquad (2.2)$$

The corresponding front and tail time constants are τ_1 and τ_2 respectively. The 200 kA lightning induces 6 kA in the support and 180 A in a power cable. The temperature rise of any of the cables is less than a degree Celsius. The Z'_t of three cables of Table 2.1 has been modeled by (2.1) for cable a and by a skin effect surface impedance approximating the data for cable b and c in Fig. 2.6:

$$Z'_t = R'_{dc} \frac{x J_0(x)}{2 J_1(x)}, \qquad (2.3)$$

with R'_{dc} the dc resistance per meter length, J_n the Bessel function of order n, $x = \sqrt{-jf/f_\delta}$ and f_δ the characteristic frequency where the skin effect sets in (see also [Ste08b]). The measured Z'_t of cable b and c is more complex than (2.3); at high frequencies the fit overestimates the measured $|Z'_t|$ (see Fig 2.6). The current has been converted into frequency domain by Fourier transform over 2×10^5 points with

Table 2.3: Model parameters of first and subsequent lightning stroke, after [IEC06]

	first			subsequent		
Parameter	I	II	III-IV	I	II	III-IV
I [kA]	200	150	100	50	37.5	25
k		0.93			0.993	
τ_1 [μs]		19			0.454	
τ_2 [μs]		485			143	

Table 2.4: Peak cable currents and voltages calculated for the first and subsequent lightning stroke, attached at point L3 (see Fig. 2.1(a)). The cable length is 100 m; propagation time and resonance phenomena are not considered.

cable	first		subsequent	
	I_p [kA]	V_p [kV]	I_p [kA]	V_p [kV]
a) 3-ld.	0.18	0.74	0.045	6.4
b) arm. 2-ld	0.18	0.25	0.045	0.34
c) fieldbus	0.12	0.11	0.030	0.032

0.1 μs time step, and then multiplied by the transfer impedances. The resulting voltage has been converted back into time domain by an inverse transform. The initial parts of the voltage waveforms are shown in Fig. 2.9. Calculated induced peak voltages are given in Table 2.4, together with the voltages corresponding to the subsequent return stroke calculated similarly (50 kA, 0.25 μs rise time, 10^6 points with 10 ns time step).

Please note that the voltages are those between the power or signal leads taken as a bundle, with respect to the PE lead or shield. The peak voltage induced in the unshielded cable a by a subsequent stroke could pose a problem for the equipment. The value is fully determind by the time derivative of the current in Eq. 2.2. All other values are within safe ranges. For instance, with armored cable b the voltage is a factor of 3 or 20 lower than cable a, for the first and subsequent stroke, respectively. The voltage between the power or signal leads is often one or two orders of magnitude lower than those calculated here [Dem87].

The values of Table 2.4 result from a direct extrapolation, neglecting travel times and resonances. The cable support is attached to the building structure through many wires, randomly spread with distances of the order of 3 m. This mesh of conducting interconnects is not included in the calculations. The local circuits resonate at frequencies of 50 MHz and up. The travel time of a current wave over the cable support and nearby building structure is about 0.3 μs, and subsequent strokes with rise time of 0.25 μs can excite resonances. Analogous to the overshoot $L - C - R$ resonator, a factor of two increase in current may be expected. A similar current increase has been observed due to ground reflections on tall buildings [Rak01]. The voltages of Table 2.4 increases less because of the different travel times inside and outside the cable. A more detailed analysis is not warranted for this model of the building. Nevertheless, the resonance excitation [Bau92] is the subject of ongoing investigations and some results are described in Chapter 3.

2.6   Conclusions

The LP system on the roof of a new plant has been tested by measurements, and the MoM model has been used to extrapolate to lightning currents. The MoM model correctly produces the current distribution between the roof grid and the skeleton. This distribution is mostly determined by the local magnetic coupling. The lightning capture rods are connected to the grid. In case of a stroke on such a rod mid-roof, the grid will be important. But in all other cases the denser and heavier building skeleton
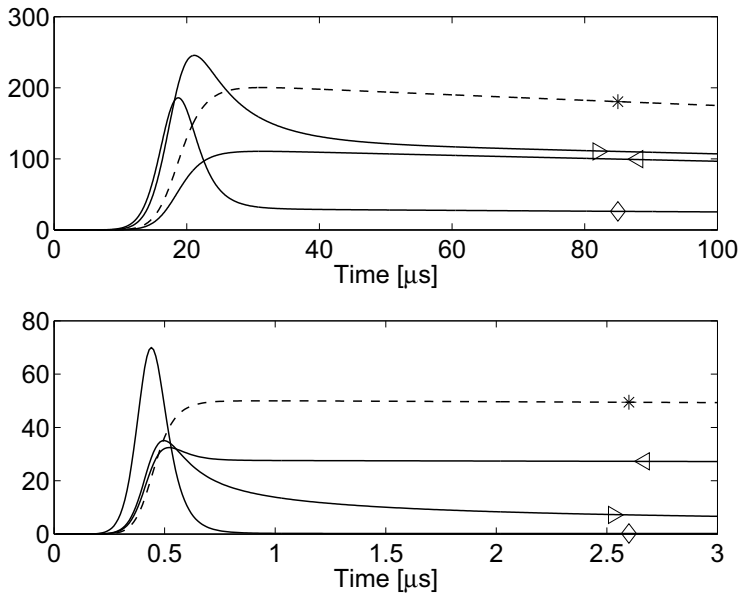
Figure 2.9: Initial part of the waveforms for current and voltage. (Top) First stroke lightning current(∗ dashed, in units of kA) and voltages on three-lead cable (⋄, divided by four), armored cable (▷), and fieldbus cable (◁). (Bottom) Subsequent stroke lightning current (∗ dashed, in units of kA) and voltages on three-lead cable (⋄, divided by 100), armored cable (▷, divided by ten), and fieldbus cable(◁). At times larger than shown by the graphs, the voltages approximately follow the current.

appears to be a better lightning protection. The model presented overestimates the cable support current by a factor of 3 when compared to the measurements; a factor of 1.6 when including the un-intended conducting air duct. Even assuming the larger support current, the cables appear well protected.

Cable bundles have been intensively studied elsewhere, see e.g. [And09]. When applied in large numbers such as in automobile industry, a large effort in the modeling is justified. In a building as discussed here, one has to accept the "as built" situation. To retrieve the actual composition of the cable bundles and the individual cable connections required a number of man-hours that was unavailable for the present study. In addition, incomplete knowledge about the building details remained, such as other metal and the interconnections. The uncertainty of the model is more due to the available input than to the MoM itself. In a comparable low-frequency calculation, where analytical expressions for the fields were available, an accuracy of better than 2% could easily be achieved [Deu09] using the same software. Still, the limited model applied gave acceptable results and good indications for the lightning safety of the installations.

The measurements on the Z_t show the benefits of armored/shielded cables even inside buildings.

A case study on lightning protection, building resonances considered

The paper [Bar10], and Chapter 2 dealt with current injection measurements to test the lightning protection system of a newly built pharmaceutical plant. The measurements were tentatively extrapolated to actual lightning. In this chapter we extend the model and calculate the response of the installation to lightning currents, and include resonances in the cable trays and test cables contained in the trays. It turned out that suspension rods between roof support and cable tray were indispensable to suppress the resonances. The time dependencies of the present results and the simplified model of Chapter 2 differ greatly, but the amplitudes of induced voltages appear to be of the same order of magnitude. This chapter is currently under review of the IEEE Transactions on Electro Magnetic Compatibility [Deu11].

3.1 Introduction

In Chapter 2 we presented current injection measurements on a newly built pharmaceutical plant that aim to verify the lightning protection scheme adopted in Chapter 2. The measurements agreed with a simplified model of the building, based on the Method of Moments (MoM) [Fek08, Fek10].

The building model consisted of three levels: the lightning protection grid on the flat roof at 19 m, the steel skeleton to carry the roof at 18.5 m and the cable support system in the fourth (top) floor, at 3 m below the roof. Downconductors and steel structures brought the lightning current to a system of grounding electrodes in the soil. In the measurements, the injected current was a damped sinusoid of 18 kHz, equivalent to a rise time of 9 μs. The roof skeleton carried 80% of the injected current, and the lightning protection grid the remaining 20%. This was also found in the MoM model. The cable support branch #1 (Fig. 3.1) carried 1.1%. The model predicted 3%, lowered to 1.7% if a nearby large diameter airduct was also taken into account as conductor.

Resonances over the 69 m wide building and support were not measured, and

therefore not considered in Chapter 2. In an extrapolation to actual lightning, this is acceptable for the first stroke with a 10%—90% rise time of 8 μs according to the lightning current wave shape proposed in [IEC06], see Appendix C. However, the subsequent stroke rises 40 times faster (0.2 μs) and will excite resonances. Four coupled resonators are then relevant for the analysis: 1) the building structure, 2) the support, 3) the cables inside the support, 4) and finally the cables internally. The half wavelength resonance in the building occurs at 0.6 MHz, and at about 2.0 MHz in the support. As will be shown in Sect. 3.3, the suspension rods between cable support and steel skeleton shift the support resonances to much higher frequencies where lightning is less important.

3.2   Model

Several models exist for the distribution of the lightning current over the channel length [Bab08a, Bab08b]. The distribution is certainly relevant for the electric fields and induced current of nearby or far away lightning. For a direct stroke on the building, the current at the point of impact is more important than the channel current at distances larger than the building size. The lightning channel is then modeled as a 200 m long vertical path, excited by a voltage source 1 m above the roof. In order to suppress resonances over the lightning path, series impedances were embedded following a profile proposed by Wu and King [Wu65]. The calculation of the serie impedances is explained in Appendix A. In the MoM model, all currents and voltages in the building are then related to the current at the base of the source. An upper frequency of 10 MHz suffices. The damping of the resonances is mostly due to the surface impedance of the conductors, and to a minor part by re-radiation at higher frequencies. The support conductors were modeled with the skin effect. For steel conductors we included the magnetic property (relative permeability $\mu_r = 200$). In order to estimate the effect of saturation, we repeated the calculation with $\mu_r = 1$ also for steel. With a step of 1 kHz, the density of frequency points is sufficient to describe the resonance damping accurately.

Fig. 3.1, an adapted copy of Fig. 2.1 in Chapter 2, shows the lay-out of the cable support. In the MoM, three parallel tubes are assumed with diameters to fit the current distribution over the actual rectangular beams (Fig 3.1a). The tube ends are connected to the local downconductors; at the junction of #1, #2 and #3, the tubes are interconnected. We consider a bundle of three test cables on the support: a) a three lead power cable, b) a twin-lead power cable with steel armor and c) a twin-lead fieldbus cable with its shield consisting of an aluminum foil and a thin copper braid. The cables follow a similar path as in the actual installation. Fig. 3.1b shows the cable positions with respect to the central beam at the horizontal distance x of 35 mm. (See also Fig. 2.8 in Chapter 2). The cables extend downward over 2 m at the near end (N) close to L3 and 13 m at the far end (F) of section #3. Their total length is 82 m.

The coupling between the MoM derived support current I_s and the cable leads and shields, is described by a mutual inductance M that depends on the position of the cables. The contribution of the support surface impedance is negligible compared to ωM (ω the angular frequency). The propagation of the transmission line (TL) modes between the cables and support and those inside the cables is described by the
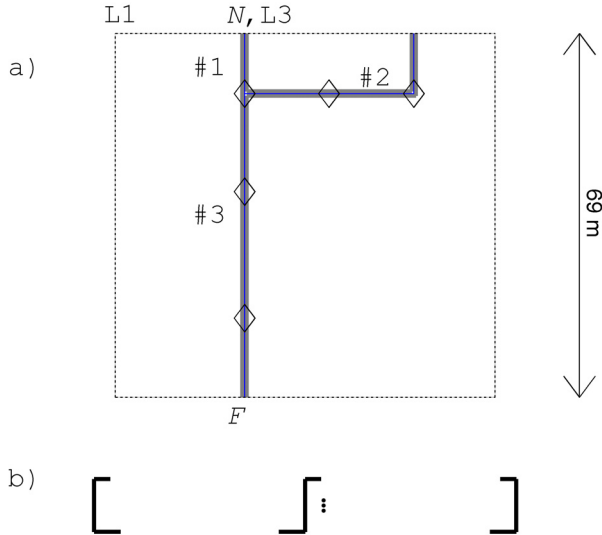
Figure 3.1: a) The support branches routing in the horizontal plane; the various points and markers are discussed in the text; b) The support cross section (100 times enlarged) where the three dots indicate the cable positions at 35 mm from the central beam.

BLT method [Bau78], or rather by the equivalent method presented in [Djo87]. We implemented the distributed coupling via M in a similar way as [Van78, Ch. 3] and [Tes97, Ch. 7], extended to multiconductor TLs, see Appendix B. The inductance and capacitance matrix for the cable shields, inner leads and support result from a quasi-static 2D calculation [Deu01a], where the three interconnected support beams act as common return. The capacitance matrix uses the known dielectric constants of the insulator materials. The cable capacitances and inductances agree with those measured for 1 up to 3 m long cable samples to within 10%. We employ analytical approximations for off-diagonal matrix elements and for the (inner and outer) surface impedances, except for the transfer impedances Z_t.

The measured Z_t of the cable shield or armor has been shown in Fig. 2.6 of Chapter 2. As the Z_t of the shielded or armored cable does not show a linear increase with frequency, even at the highest frequencies near 20 MHz, the skin effect on the wires in the aluminum foil, braid or armor dominates over the magnetic coupling through the holes in the braid. We conclude that it is also justified to neglect the capacitive coupling Y_t compared to skin effect Z_t. As in Chapter 2 we use the analytical approximation with Bessel functions, describing $|Z_t|$ within a factor of 2 and the phase within 10 degrees.

For shielded cables, the natural mode currents flow in the inner loop (differential mode: inner conductor and inside of shield as return) and the outer loop (common mode: outside of shield and support as return) [Hel95b]. The TL formulation in [Djo87] uses the net current through each conductor. The transformation of currents, voltage and impedance and admittance matrix between the two descriptions has earlier been presented in [Dem00].

Table 3.1: Parameters for IEC class I lightning current.

	I [kA]	k	τ_1 [μs]	f_1 [kHz]	τ_2 [μs]	f_2 [kHz]
first	200	0.93	19	50	485	0.33
subseq.	50	0.993	0.454	$2 \cdot 10^3$	143	1.1

We choose two lightning strike positions, L1 at the corner of the building and L3 at about 1 m towards L1, near the conduit end N (Fig. 3.1). The calculation starts with the determination of the distribution of the current I_s as sum over the three support tubes for the frequencies 1 kHz up to 10 MHz. In the MoM software FEKO, the maximum length of the elements is 1.5 m and the total number is about 3000. In a postprocessing step, the distributed M-coupling to the TLs is calculated. The P and Q integrals [Van78, Eq. 3.4] are determined as a sum over the elements, with the series distributed voltage source $E_z = j\omega M \cdot I_s$. In the TL model, all cables conductors are short circuited to the support at the far end F in Fig. 3.1, where far is regarded from the lightning attachment point. This was also the case in the experiments in Chapter 2. At the near end N, the shield, the ground lead and the armor are again shorted to the support. For each frequency we determined the transfer between the source current on one hand and the cable currents to the support near N and F plus the voltage between the open ended leads and support at N on the other hand. As final step, the lightning current is considered. We assume the IEC model, shown in Appendix C and [IEC06], with the highest severity class I. The time dependence of the lightning current is

$$i(t) = \frac{I}{k} \times \frac{(t/\tau_1)^{10}}{1 + (t/\tau_1)^{10}} \exp(-t/\tau_2), \tag{3.1}$$

with parameters given in Table 3.1. The spectrum of $i(t)$ is constant below the frequencies f_2, rolls off $\propto 1/f$ until f_1 where the decay becomes much steeper. The Fourier transform of $i(t)$ is multiplied by the transfer functions mentioned above, to give the response spectra. The response spectra are complex conjugated and mirrored with respect to the maximum frequency of 10 MHz to facilitate fast Fourier transform. We interpolate the spectra into a mesh with 50 Hz steps, to allow a large time domain. The inverse Fourier transform then provides the time dependent currents and voltages near end N.

3.3   Results

The results for a lightning stroke at a sensitive point, the top of the conduit system (L3 in Fig. 3.1), are presented first. We discuss the results for a stroke at building corner L1 later.

In an introductory calculation, the support and the steel skeleton were only interconnected at the support ends, thus forming an extended resonator with a large quality factor. The first resonance occurred at 1.96 MHz as shown for branch #1 in Fig. 3.2b. The oscillatory grey line represents the branch #1 current, in case of excitation by a subsequent stroke at L3. In the actual installation, the support is

suspended from the skeleton by a large number of rods irregularly spaced at about 2 m distance. The electrical contact between rods, skeleton and support is present but is not guaranteed. We choose to model this situation by 5 rods (⋄ in Fig. 3.1a) which shifted the first resonance upwards to frequencies where the lightning current contributes less. Fig. 3.2a shows the resulting current transfer from source to support branch #1 close to the junction. Below 1 MHz, the transfer is approximately 0.04 and constant. At these frequencies, the current distribution in the building is governed by induction Sect. 3.1. The transfer rises approximately proportional to frequency above 1.6 MHz; some resonances are present. For the 200 kA first stroke at L3, 4% of the current flows through branch #1, in reasonable agreement with the 2.5% mentioned in Chapter 2. The support current has the same wave shape as the lightning current, since the whole building has a dominant inductive behavior below 1 MHz. The smooth line in Fig. 3.2b shows the response to a −50 kA subsequent stroke. It exhibits only minor oscillation on this scale.

In the support of the actual installation, the cable position varied (see Fig. 2.8). We therefore compare two extreme positions: 35 mm from the central beam, and 200 mm, which is midway between the central and right beam. The M varied by a factor of 3, 23 and 69 nH/m respectively. The cable currents and voltages varied by a factor of 3 or less because of the accompanying change in TL matrices. In case of a first stroke, the cable currents resemble the lightning current waveshape, but differentiated because of the $j\omega M$ coupling between support and cables. Therefore, we only give the peak values in Table 3.2. The cable currents are less than assumed in Chapter 2, mostly since the current through branch #3 of the support is less than one half of the current through branch #1, and 84% of the cable runs over branch #3. As a result, the voltages are also smaller than in Table 2.4.

In case of a subsequent stroke, current and voltage for the 3-lead cable are shown in Fig. 3.2c and d. Since the oscillating behavior is dominant, we present half of the peak to peak values in Table 3.2. The fieldbus cable behaves in a similar manner, with adapted amplitudes for current and voltage (Fig. 3.2e), as does the common mode current through the armored cable. However, the large damping by the armor causes the differential mode voltage to decay much faster, to within less than 10 μs.

We tested the saturation effect, by assuming a relative permeability μ_r of 1 for the steel support. The changes with respect to $\mu_r = 200$ were negligible.

The effect of a power line filter with an assumed 2 nF input capacitor has also been considered. For the subsequent stroke, the voltages on the 3-lead and armored cable are reduced by a factor of 2 and 6 respectively. The cable common mode currents are not affected. For the first stroke, there is only a small reduction, if any at all.

When the current is injected at the point L1 instead of at L3 (Fig. 3.1), the support current pattern completely changes. Cable currents and voltages decrease with a factor varying between 4 and 2.5 for both first and subsequent stroke; see Table 3.2.

The last row of Table 3.2 gives the values for the cable current and voltages when the cable support is allowed to form a resonating structure with the roof skeleton. Current and voltages are more than a factor of 2 too high compared to the model with connections between the cable support and roof skeleton.

Table 3.2: Cable current and voltage calculated for the first (F, peak current and voltage) and subsequent (S, half of peak to peak values) lightning stroke, attached at point L3 or L1 (Fig 3.1a). The last line (S*) shows the data omitting the suspension rods in the model.

Pos.	F/S	3-lead		armored		fieldbus	
		I	V	I	V	I	V
att.		[A]	[kV]	[A]	[kV]	[A]	[kV]
35	F (p)	8	0.07	14	0.03	19	0.04
L3	S (p-p)/2	7	1.4	11	1.4	13	0.07
200	F (p)	23	0.16	28	0.05	43	0.09
L3	S (p-p)/2	17	2.7	21	2.2	31	0.16
35	F (p)	3	0.02	4	0.01	6	0.01
L1	S (p-p)/2	6	0.8	8	0.6	9	0.04
35	S*(p-p)/2	24	3.7	41	3.2	40	0.13

3.4 Discussion

The lightning current waveform has two roll-off frequencies mentioned in Table 3.1. The mutual inductance coupling $\omega M'$ between support and cables rises with frequency. This cable current remains limited by the selfinductance L' of the cable inside the support. The roll-off is counteracted by the increase of the transfer to the support current with frequency, at least up to 8 MHz; see Fig. 3.2a. But when the cable length becomes comparable to a quarter wavelength, averaging over the cable length sets in and further increase of the cable current is halted. The Z_t of the 3-lead cable rises with f above a few kHz, the one for the armored cable rises with $\omega^{1/2}$ above 4 kHz, as does the one for the fieldbus above 200 kHz. The large voltages for the 3-lead cable and the armored cable are caused by the increasing Z_t rather than by the larger common mode currents. All internal cables circuits are open at one end; the odd multiples of the first quarter wavelength resonances of the armored and fieldbus cables are clearly less pronounced in Fig. 3.2c–e.

It is interesting to compare the results with the simple model summarized in Table 2.4 where resonances were neglected, even though the situations are different. In Chapter 2 the current ratio is based on the 18 kHz measurements and this ratio is used to determine the current in the gutter and cables. In this chapter we assume the position of the cables in the support to be invariable, although it varied in the actual building. The cable currents of the model presented here are smaller than the values assumed in Chapter 2. As a result, the voltages for the 3-lead cable are smaller by a factor of about 5. The same holds for the armored cable, but only in case of the first stroke. For the subsequent stroke the voltages are larger than those from the simple model of Chapter 2. This is tentatively attributed to the rise of $|Z_t(\omega)|$, but remains an item for further investigations. The voltages on the fieldbus cable are comparable or a factor of 2 larger.

We used the IEC level I lightning current waveshape, whereas for the building modeled level III with half the amplitudes was requested.

Several other assumptions than mentioned before have implicitly been made in the analysis. We neglected pigtails at the points where the cable leave the support towards the equipment. Similarly, all other cables on the support (Fig. 2.8) have not been considered, because of lack of information about their paths and common mode currents. Also the influence of other conductors on the support current has not been taken into account. As shown in Chapter 2 the nearby airduct reduced the support current by a factor of 1.7. The twist of the leads in the cables has not been considered in the calculations. However, twisting would not reduce the coupling between the unbalanced cables and the support current. This is particularly true for a 3-lead cable.

3.5   Conclusions

The benefit of a continuous and interconnected cable support is clearly demonstrated by the present lightning protection model. Many distributed short circuits between support and skeleton suppress low frequency resonances, and improve the lightning protection. The calculated values of the currents do not damage the cables thermally, see Chapter 2 Section 2.5; the voltages are in a range that passive filter components can handle.
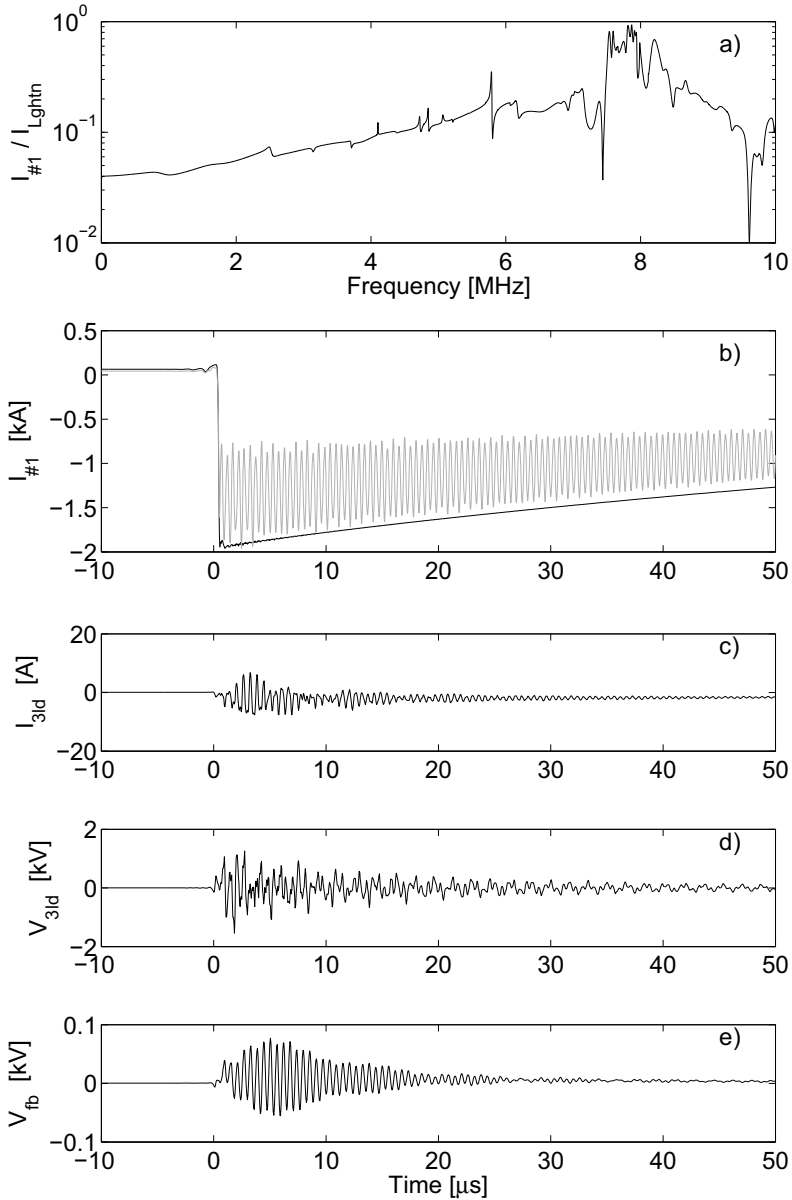
Figure 3.2: a) Transfer of source to support branch #1 near the junction (Fig. 3.1);
b) Solid line: current in support; c) and d) Current and voltage for 3-lead cable at
the near end with the cable bundle at 35 mm from the central beam; e) the voltage
for the fieldbus cable. The data in b) up to e) assume a subsequent stroke at L3
(Fig. 3.1).

Chapter 4

Lightning protection improved by multiple interconnects in buildings

Two simplified models for a large building are compared for their lightning protection properties, one without and one with interconnecting conductive elements. The dimension is 69×19 m. At frequencies below 2 MHz, the additional elements provide a skin-effect like protection of the building interior. The benefits of the interconnections at high frequencies are the suppression of resonances and shifting these to still higher frequencies where lightning is less prominent. This chapter has been accepted at the EMC Europe conference of 2011.

4.1   Introduction

Lightning protection of buildings remains an subject of interest studied by different modeling techniques. Often, the model is quite simplified or even reduced to the outer skeleton. For instance: [Miy08]. For large or tall buildings, the travel time over the structure can become comparable to the rise time and resonances show up. This is especially true for the subsequent stroke with a rise time of the order of 0.2 μs [IEC06] and Appendix C. The resonances are often related to the model rather than to the actual building. In this contribution we compare an over-simplified structure with one containing additional interconnecting elements, cross beams, rods etc. Their effect is to shift the resonance frequencies upwards, to regions where lightning contributes less.

4.2   Building model

In a previous study, we investigated the lightning protection of a $69 \times 71 \times 19$ m pharmaceutical plant by measurements and by modeling in the Method of Moments (MoM) (Chapter 2,[Bar08],[Fek10]). A diagram of the model is shown in Fig.4.1. From the roof downwards, three layers were considered: the copper protection grid
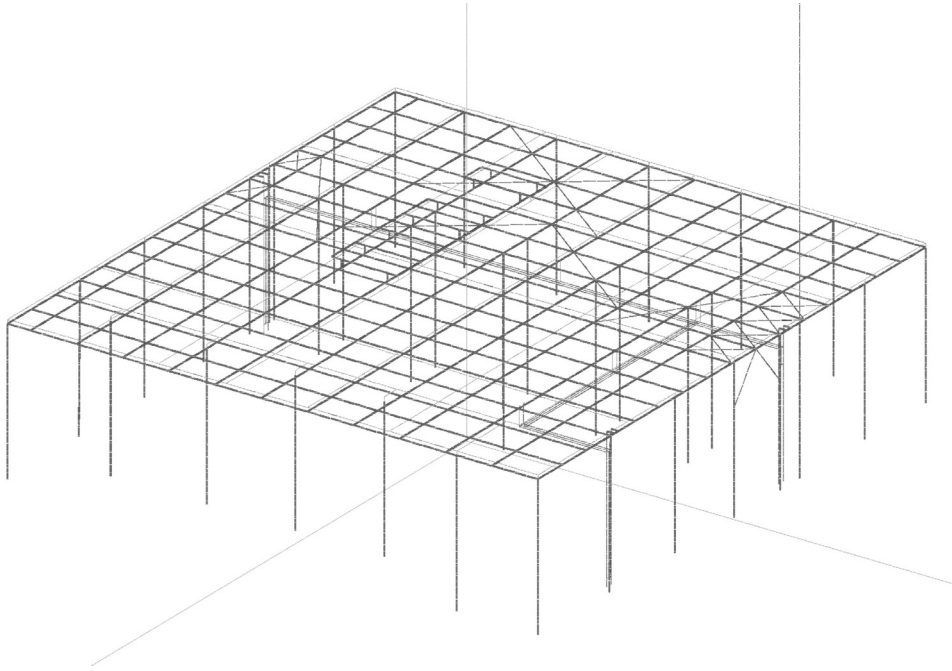
Figure 4.1: Model of the $69 \times 71 \times 19$ m pharmaceutical plant. The rightmost vertical dashed line indicates the 200 m tall lightning channel. Please note the conduit system inside extending over the full width of the plant.

with poles to capture the stroke at 19 m height, the roof supporting steel beams 0.5 m lower and a single steel cable support conductor at 3 m below the roof grid. This model structure proved to be a sufficient representation for the purposes of the experiment, where we measured current and voltages on test cables in this cable support. The model is certainly not complete yet, but contained the tested electrical installation and its cabling on the fourth floor.

All cable ladders and trays in the support were interconnected and connected to the lightning protection structure and down conductors. In line with the wording of [IEC97] and to avoid confusion with the roof supporting skeleton, we use the term "conduit" for the cable support. In the measurements, a capacitor discharge delivered the current in the grid; the current returned through two guy wires and ground placed electrodes at some distance of the building. The measurements and the Method of Moments (MoM) model agreed on the current distribution between the roof grid (20%) and the steel structure (80%). At a point near the wall of the building, the conduit carried 1.1% in the measurements. The MoM model with the capacitor source resulted in 3%. A 1 m diameter airduct was present parallel to the support. If this duct was also considered as a continuous conducting structure, the conduit current part lowered to 1.7% in the MoM model. There is little doubt that additional parallel conductors would have further reduced the calculated part of the conduit current.

The purpose of this chapter is to present the benefits of additional vertical interconnections for the lightning protection. In a simpler structure than the building of
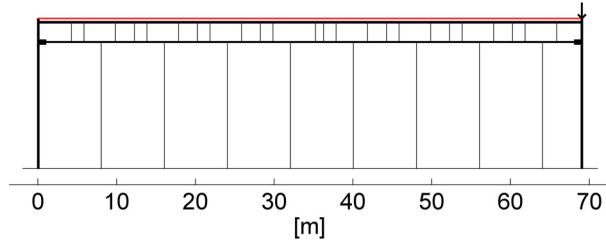
Figure 4.2: Simplified model of the structure as considered. From top to bottom, the horizontal conductors are the roof grid, the steel roof skeleton, the conduit and the ground, assumed perfectly conducting. The heavy lines parts indicate the elements 1 and 69 of the conduit. The arrow indicates the base of the 200 m tall lightning channel. The thin vertical lines are interconnections skeleton—conduit and conduit—ground.

Fig. 4.1 we retain the three levels. In order of increasing height we have a single conductor for the roof grid, one for the steel skeleton and one for the conduit. Two down conductors are assumed at the building walls (heavy lines in Fig. 4.2). This cross section of the building is the arch model. The soil is regarded as an ideal conductor. Three coupled resonators are thus formed: the support and the ground, the support and the roof skeleton, and the skeleton together with the conduit. First we assume no interconnections and calculate the current distribution over the arch assuming a long vertical path as a lightning channel energized by a source at its base. Later on we add the interconnections (thin lines in Fig. 4.2), and calculate the current distribution again.

4.3   Lightning channel model

We introduce a 200 m long vertical current path at the top-right corner to represent the lightning channel. The channel is excited by a voltage source at 1 m above the roof. Such a long channel would also resonate near frequencies where the length is equal to odd multiplies of a quarter wavelength. In order to avoid the channel resonances, series impedances are introduced according to a profile suggested by Wu and King [Wu65]. In the MoM, the maximum length of all current path elements is 1.5 m. The frequency ranges from 1 kHz up to 10 MHz. IEC documents [IEC06] describe the time dependence of the lightning current stroke $i(t)$ by the same mathematical form for the first and the subsequent strokes. The so-called Heidler model [Hei85] is:

$$i(t) = \frac{I}{k} \times \frac{(t/\tau_1)^{10}}{1 + (t/\tau_1)^{10}} \exp(-t/\tau_2). \tag{4.1}$$

Table 4.1 gives values for the parameters for the both strokes, assuming a class I severity according to IEC. The wave shape and spectrum of $i(t)$ is given in Fig. 4.6, where we indicated the two cross-over frequencies f_1 and f_2. The spectrum of $i(t)$ is constant below the frequencies $f_2 = 1/2\pi\tau_2$, and then rolls off as $1/f$ until f_1 where the decay becomes much steeper (Fig. 4.6). An upper frequency of 10 MHz is sufficient for the subsequent stroke, since the spectrum is then down by a factor of more than 10^4 with respect to the DC value.

Table 4.1: Parameters for IEC class I lightning current.

	I [kA]	k	τ_1 [μs]	f_1 [kHz]	τ_2 [μs]	f_2 [kHz]
first	200	0.93	19	50	485	0.33
subseq.	50	0.993	0.454	$2 \cdot 10^3$	143	1.1

4.4 Model response

We calculated the current distribution in the arch model, as a function of frequency. The skin effect on the elements is included in the model. For steel and copper we assumed standard values of the resistivity $\rho = 10$ and 1.7 $\mu\Omega$cm respectively; the magnetic permeability of steel is chosen at $\mu_r = 200$. With this parameters, a step of 1 kHz provides a sufficiently dense frequency mesh to describe the resonances and their damping.

4.4.1 Original arch structure

The transfer of the source (lightning) current to all other elements stems from the MoM output. For the actual building, the current in the cable support is of special importance. Here, we judge the effectiveness of the lightning protection by the current in the first conduit segment, as viewed from the rightmost downconductor that is topped by the lightning channel. This is the right heavy accentuated conduit section in Fig. 4.2. Fig. 4.3 shows the transfer $T_1(f)$, which is the current in the first conduit element, divided by the source current, as a function of frequency. The transfer is quite flat up to about 0.5 MHz, and equal to about 0.08. The phase angle is near to zero. This is the frequency range where the current distribution is determined by inductive effects inside the building.
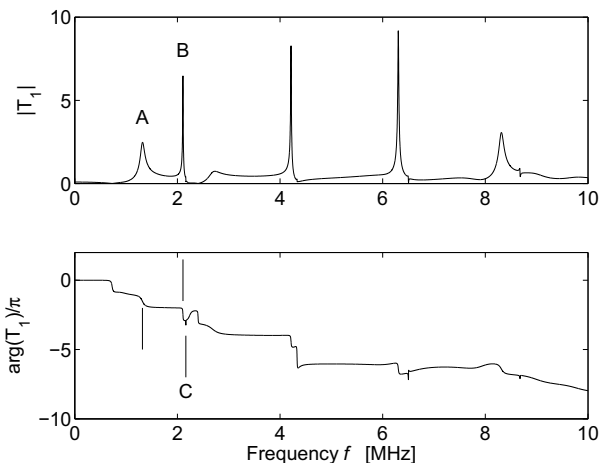

Figure 4.3: Absolute value and phase of the transfer T_1 between lightning current and conduit element 1 in the arch model of the pharmaceutical plant.
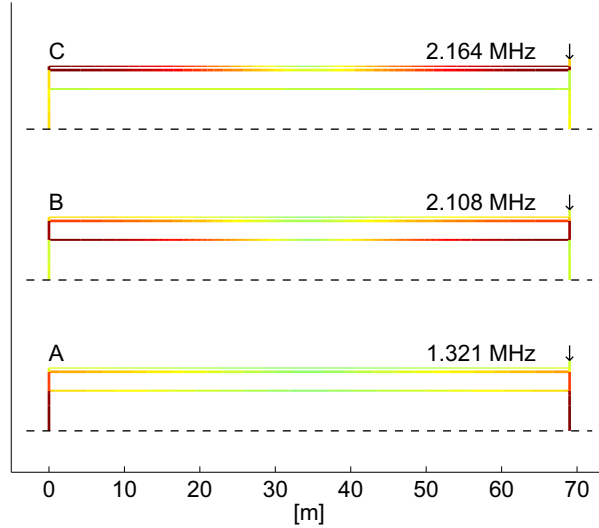
Figure 4.4: Current amplitudes over the structure, for the resonances A, B and C. Red is indicating a maximum and via orange/yellow going down to minimum green.

Three fundamental resonances shown up, indicated by A, B and C, at the frequencies 1.321, 2.108 and 2.164 MHz respectively. The vertical lines in the phase plot repeat the positions of A and B. In the amplitude plot, the small resonance C is barely visible as a shoulder on resonance B, but it is better recognized as a sharp dip in the phase plot. Up to four harmonics of the resonances are seen in Fig. 4.3. The current patterns of the fundamentals are shown in Fig. 4.4, with the color scaled between the maximum transfer $|T_1|$ and the value of zero. The current varies only little over the downconductor length. In order to save space, the downconductors are shrunk by a factor 3 below the conduit. Resonance A has the current in the loop formed by the soil, down conductors and the bundle of roof grid, skeleton and conduit together. This resonance appears well damped; the large area of the loop formed by the downconductors, conduit and soil ensures that this loop is an efficient radiator. The current loop for resonance B is the transmission line between the conduit and skeleton; for C, the one between skeleton and roof grid. Loops for B and C are less damped as is apparent from their smaller spectral width, since these are less efficient radiators.

Fig. 4.5a shows the corresponding time response of the conduit current on the first element, on a subsequent stroke with an amplitude of 50 kA. The oscillatory response is clear and consists mainly of resonance A. It is superimposed on a waveform that resembles the lightning current (Fig. 4.6) multiplied by the factor of 0.08 mentioned above.

4.4.2 Cross beams and additional poles

A building usually contains many more conductors such as vertical poles or supports. We added a number of cross-connections, shown by the thin vertical lines in Fig. 4.2.
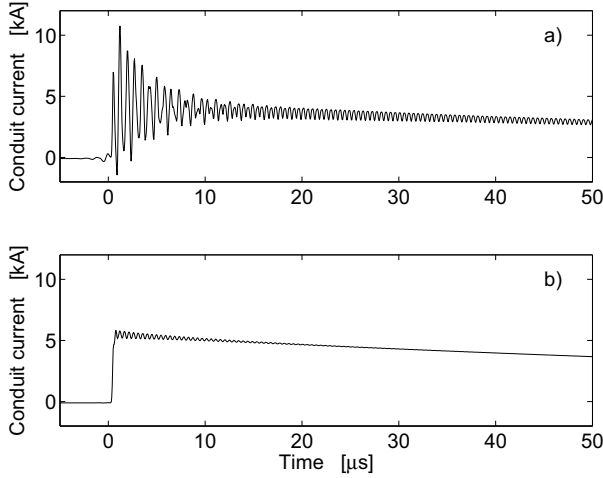
Figure 4.5: Conduit current near the downconductor struck by a subsequent lightning stroke, for the arch model without (a) and with (b) additional vertical conductors.

Current is brought to the conduit via the connections with the steel structure, and removed again via the additional ground connections. The response as function of frequency, again judged by the first conduit element T_1, is given in Fig. 4.7. Also here, the low frequency transfer T_1 is of the order of 0.08 at zero phase angle. At the other end of the conduit, $|T_{69}|$ is a factor of 30 less. As a function of position over the conduit, the interconnections to ground cause an average exponential decay over the length with a decay length of about 23 m. This is equivalent to a reduction factor 1.5 per ground connection.

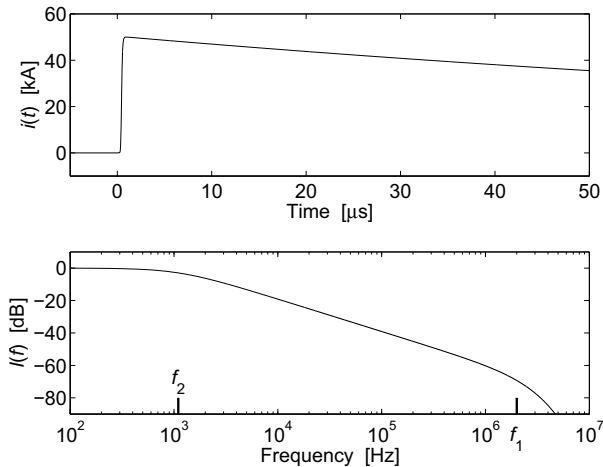At higher frequencies the response is smaller and less peaked below 8 MHz. The

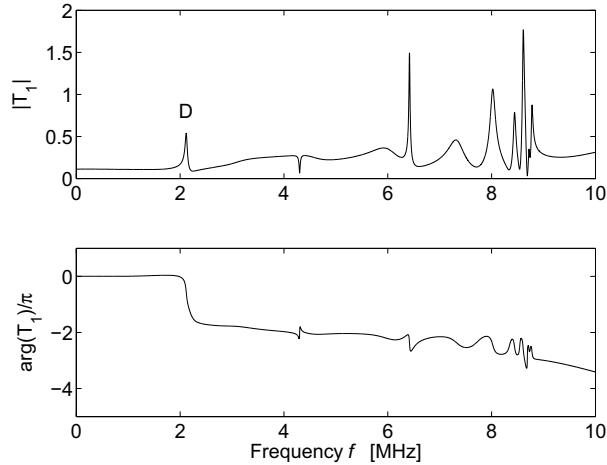Figure 4.6: Time dependence and relative spectrum of subsequent lightning stroke

Figure 4.7: Absolute value and phase of the transfer T_1 between lightning current and conduit element 1 in the arch model with additional interconnections (Fig. 4.2).

single resonance D at 2.117 MHz replaces the A, B, and C of the previous case. The corresponding current distribution over the structure is less clear than in Fig. 4.4. Above 8 MHz additional resonances show up (half wavelength equal to building height). The time domain response T_1 (Fig. 4.5b) shows only little oscillations.

4.5   Discussion

Additional interconnections reduce the current through the cable support (conduit) and shift resonances to higher frequencies. In actual buildings, many more conduit suspension points cable on the roof structure are likely; however, their conduction is not guaranteed as these suspensions are primarily of mechanical interest.

The coupling between the support current and the cables inside the support of predominantly inductive for the frequencies considered here. A mutual inductance M' between cable and the net conduit current can be introduced Chapter 2, as well as a selfinductance L' of the loop formed by cable and conduit. The cable current is then limited to the fraction M'/L' of the net conduit current. That fraction is usually much smaller than 0.1.

The final voltages in the cable scale with its transfer impedance Z_t'. An unshielded three lead power cable has Z_t' proportional to frequency over the relevant range. For a shielded or armored cable, Z_t' rises proportional to $\sqrt{f}$, see Chapter 2 section 2.3 and Fig. 2.6. The Z_t' rise partly cancels the decay in the lightning current spectrum. Different travel times of internal and external waves, however, cause a decay in effective coupling length, when a quarter wavelength becomes smaller than the cable length. This occurs near 1 MHz in the case considered here. A model including the full pharmaceutical plant and the travelling wave effects is discussed in more detail elsewhere [Deu11] and Chapter 3.

Although not investigated in this study, an irregular placement of pillars and other

interconnects frustrates the higher frequency resonances to build up and thereby reduces the lightning coupling. However, such an approach might conflict with architectural requirements.

4.6 Conclusion

Additional interconnects cause a reduction of lightning current inside the building, resembling the skin effect. They also reduce the excitation of internal building resonances and shift the resonance frequencies upwards. Models for the lightning protection of buildings should be extended enough to include a sufficient number of such interconnects to avoid unrealistic artefacts.

Chapter 5

Lightning protection measurements

The lightning protection of various industrial installations has been investigated by injecting current of smaller amplitudes. In this chapter two of these installations will be examined and this will give insight in measurement results with to many unknowns to derive a model. The contents of this chapter is published as a part of a conference paper [Bar08]. The tekst of this chapter is adapted for this thesis.

5.1   Introduction

For high-risk objects or objects with large economic value it is advisable to test the protection by current injection. Ideally the current should have sufficient amplitude and sufficiently short rise time comparable with real lightning. Such an approach is followed for instance for airplanes in the certification trajectory. For large size buildings, or industrial installations, the amplitude is difficult to attain [Die85b] and [Die85a]. But in systems where the major part of the protection is provided by metallic conduction, the protection system behaves linearly to a high degree. The primary requirement on the test current then becomes a short rise time such that the system inductive behavior is properly assessed [Mon98], [Laa98] and [Mar02]. The linearity ensures that injection tests with lesser amplitude can be extrapolated. But more importantly, the amplitude can be chosen low at the begin of a measurement cycle, to reduce the chance that sensitive and possibly expensive equipment installed in the building under tests is damaged by the tests. However, there always remains a risk that real-lightning arcing over barriers modifies the current path compared to the tests, and thereby the protection. This aspect has to be considered carefully.

5.2   The two buildings

Two short one-day measurements on the lightning protection of industrial buildings are described. These measurements where on request and to answer specific questions. The building of the first test is an existing structure of steel beams with steel risers. Steel window frames were mounted in brick facade elements. The building
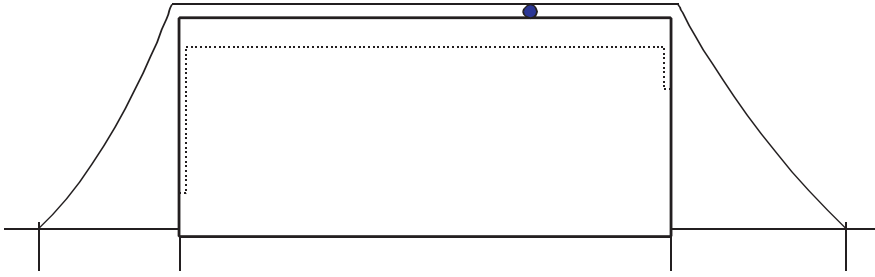
Figure 5.1: Schematic diagram of injection circuits. The dot on the roof indicates the source position, the dotted line indicates the path of the cable ladder in the building

is about 6 m high, but covers a large area. At the time of construction no further dedicated lightning protection was installed. In the building large electronic systems are investigated in the final stage of development. Cables for signal and power ran via metal conduits mounted against the vertical risers. The protection became a serious concern after a lightning strike event on this building. The direct damage was limited to a few desktop computers. But the indirect damage was a major problem: over an appreciable time system failures were attributed to the after-effect of the lightning. In a series of retrofitting actions a lightning capture grid was installed on the roofs connected to individual grounding electrodes. The variety and variations of electronic systems to be tested, the speed of system replacement, and the large size of the building made it difficult to implement a "zoning scheme" based lightning protection [IEC06].

The second building on the same premises was made of reinforced concrete. It had also been equipped with a roof grid. Down-conductors of 50 mm^2 copper connected the grid at regular distances of about 15 m to 11 grounding electrodes. The grid was supposedly insulated from the building. One test room was equipped with an internal lightning protection (ILP), a ring structure of 50 mm^2 copper. The ring was connected to all metal piping penetrating the room walls. A nearby room without ILP was selected for comparison. Since the rooms were intended for test of X ray equipment, all surfaces were covered with lead. Both rooms were on the second floor, in the center of the three story building.

5.3   Injection system

The current source is a 0.5 μF, 40 kV capacitor, discharging via a spark gap into the circuit formed by the lightning protection system, long Filotex high-voltage leads, and one or two additional grounding electrodes positioned at some distance of the building; see Fig. 5.1. A 27 μH coil in series with the capacitor limit the current in case of an inadvertant short circuit; see Fig. 5.2. The circuit resonates usually at 20 to 30 kHz, with a Q-factor mostly determined by the electrode resistance. Typically the current amplitude is chosen at 200 A, at the capacitor charging voltage of 3.5 kV. The current varied less than 10 percent between discharge cycles. Although each discharge has been monitored, an average current value was often assumed in
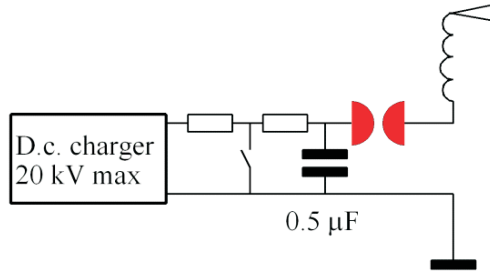
Figure 5.2: Schematic diagram of the injection source. The capacitor of 0.5 μF and the coil and spark gap are shown.

the analysis. In order to ensure linearity, the currents are measured by air-core Rogowski coils combined with active/passive integrators. In case of smaller currents we also use Pearson and Fischer current probes. For voltage measurements we use standard probes and battery-powered digital scopes. The bandwidth of the current measurements are two up to a several hundred kHz, sufficiently large to accurately record the transients.

5.4   Measurements

In the first building with the steel frame, about 32 percent of the injected current $I_i nj \approx 200$ A descended through various facade elements near the injection circuit. The remaining 68 percent could not be retrieved in the time allowed for the measurements. In spite of the magnetically open structure, the current through vertical and horizontal construction elements and conduits inside the building were remarkably low, a fraction of 1 %. We tested the protection effectiveness for a UTP cable, laid in an 80 m long predominantly horizontal metal tray inside the building. At the end deep inside the building all leads in the cable were shorted to the local 'ground'. At the other end -near the facade- we measured the open loop common mode (CM) voltage of 6 V peak and the short circuit current of 1 A peak. From these values the mutual inductance M of the loop formed by the cable and the grounding in the building on one hand, and the injection circuit can be retrieved, as well as the selfinductance L_c of the loop formed by the cable and tray. We arrived at $M = 0.35$ μH and $L_c = 53$ μH. The L_c value is quite reasonable for such a long cable. If M X d$I_i nj$/dt is extrapolated to real lightning (10^{10} to 10^{11} A/s), the induced CM voltages are 5 kV or 50 kV, likely too large for the insulation level in an ethernet connection. Because of these large values, we did not consider the common to differential mode conversion of this particular cable in detail.

   In case of the *second building* we injected a current $I_{inj} \approx 250$ A peak into the

roof grid above the test-rooms. The half-period of the pulse was about 2×10^{-5} s, and dI/dt about 4×10^7 A/s. We retrieved only 20 percent of the injected current in the down-conductors near their electrodes. The supposedly insulated grid had good connections to other metallic elements in the building. The major 80 percent part of the current flew through lesser known paths, most likely through metal stairs and elevator shaft of the adjacent and connected building. In principle this could have been determined in an extension of the measurement period, but this was not done.

The largest current found through the ILP was 0.4 A peak, as is shown in Fig. 5.3. This is 0.16 % of the injected current. Similar currents were found in the tubing for compressed air and water that entered the room. The voltages were more difficult to measure because of local high RF interference. We used a passive low-pass filter with a roll-off at 32 kHz. Its 50 Ω input impedance loaded the low-impedance ILP only slightly, some correction should be applied to measured peak voltages. Fig. 5.3 also shows the recorded voltages between a power outlet safety earth and the nearest (less than 0.5 m distance) ILP bar for two situations. First we measured the voltage with an additional connection between protective earth (PE) connection and a point on the ILP at the distance of 2.5 m. To within the measurement accuracy this voltage was the same as without such a connection. Expressing the voltage in terms of the mutual inductance, one finds $M \approx 2$ nH. Secondly, the connection was made to a point on the ILP at 0.5 m distance. The voltage reduced by a factor of 10. Extrapolated on the basis of $M \times$ dI_{inj}/dt, the "open loop" voltage corresponds to 0.2 kV. No current measurements could be performed in the non-protected test-room, because there was no equipment or installation present. Only the voltage between a far away (5 m) lightning protection rod in the corridor and the power outlet safety in the room could be measured. This voltage was even smaller than in the test-room with ILP. The lead plates in the room walls reduced the magnetic field to such low values that no proper comparison between the rooms could be made.

5.5 Discussion

Both buildings were existing, and an upgrade would have required complete refurbishing. In particular for the second building, this was not feasible. The intended lightning protection for both buildings looked similar in appearance. In both cases the downconductors contributed only slightly. Still, one would have expected that the current preferred to flow through conductors closest to the leads from the capacitor to the grounding electrodes, thus minimizing the magnetic flux. This was not observed. In view of the limited number of conductors, a method of moment based model for the steel skeleton building looks feasible. This has not been done for this building, but results of such an approach were presented in the previous chapters. The second building has too many unknowns to allow detailed calculations.

The extrapolated voltages showed the need of further measures in the first building with the steel skeleton structure. Shielded twisted pair cables would be an effective countermeasure. The reinforcement of the second building turned out to give an adequate protection. The benefit of the ILP ring in this building is unproven, if there is any at all. Remarkably, the ILP ring was not connected to the PE in the power cables. This connection could have provided some benefits.
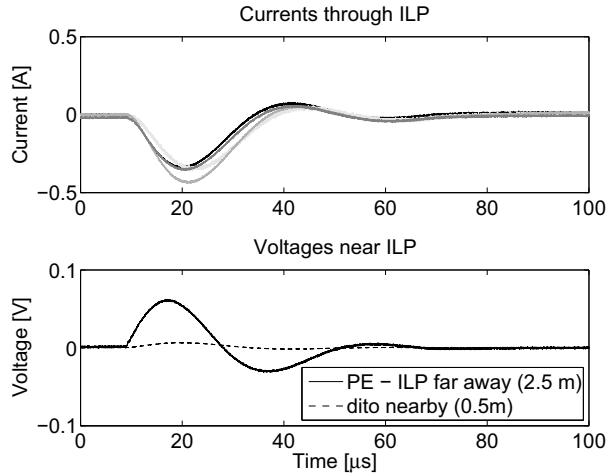
Figure 5.3: Top: several currents through the ILP measured at different positions in the protected room of the second building. Bottom: voltages measured between ILP and PE (0.5 m, dashed line) and far away (2.5 m, solid line). The voltages appear to be in phase with the current, due to the low-pass filter (see 5.4).

5.6 Conclusion

A few days current injection measurements can resolve specific questions concerning lightning protection. In fact, the method is a scaled version of bulk-current injection for equipment. The extrapolation of the data to real lightning depends on a) the scaling with I_{inj} or dI_{inj}/dt depending on the behavior of the transfer impedance Zt with frequency and b) the linear behavior of conductors, cables trays and shields. In all discussed buildings the metal structures were more important for lightning protection than the 50 mm^2 copper conductor.

Lighting test on an electronic lamp driver

Public lighting in a recently established industrial park consisted of a large number of poles with gas-discharge luminaires controlled by electronic drivers. A lightweight construction was chosen for the lampposts, made of composite material instead of metal. After two months, an unacceptably large percentage had failed which was attributed to nearby thunderstorms. The question arose whether simple remedies could be found such as improved cabling in the posts, or whether all drivers should be replaced. In a series of tests, the level of severity was increased slowly, in order to establish the limit without sacrifying many drivers. A common mode (CM) current of 100 A likely damaged the original electronic driver, a typical outdoor product (TOP). A newer generation of drivers called "Cosmopolis Extreme" (CPO Xt) was designed to withstand much higher currents. We did not damage any in our tests, even with a long spark test of 2.5 kA directly from the 2 MV lightning surge generator (LSG). This chapter has been published as a conference paper [Deu10]. This chapter is adapted for this thesis.

6.1   Installation

6.1.1   Details of power distribution

Some details about the actual installation deserve being mentioned here. The wiring inside the 15 m tall lampposts consists of two unshielded leads. All CM current to charge and discharge the lamp flows through the leads, which are in addition exposed to the lightning fields. The 230 V power arrives through two single lead cables buried in the soil, the neutral grounded at the feeding point in a TT-configuration. The cables are individually armored by two 0.3 mm thick steel foils with 100% coverage. The steel armor is again insulated with respect to the soil over the length of the cable. Over the length of the cables a horizontal bare 35 mm^2 copper ground wire is buried in parallel. At each pole, steel armor and ground wire are interconnected and
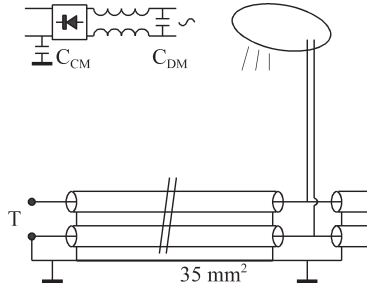
Figure 6.1: TT power circuit of the actual installation with two parallel armored cables and 35 mm^2 Cu ground wire. The inset shows the CM filter consisting of the coupled coils and C_{CM}

connected to a grounding electrode.

6.1.2 Transfer impedance of the power cable

The transfer impedance Z_t of the brand A cable is the voltage induced between inner lead and steel armor, per meter length and per ampère. The Z_t has been measured in the laboratory with the aid of a FRA5097 impedance meter by NF (Japan). Fig. 6.1 compares the brand A Z_t with the one of a brand B with an armor of woven steel wires in parallel to a copper strand inside the armor. The steel foil armor in the brand A cable causes a large Z_t. We did not study possible effects of magnetic saturation of the steel at high current.
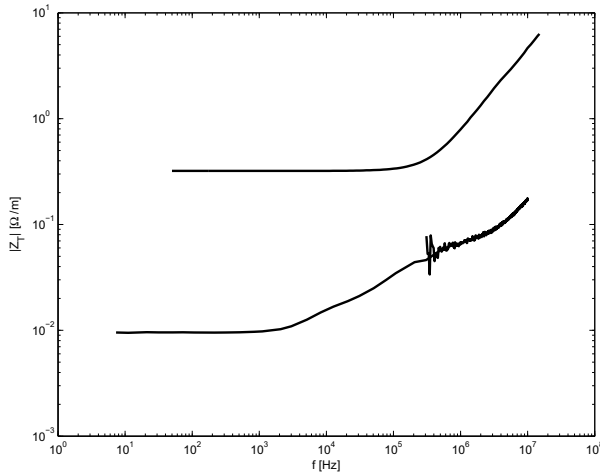

Figure 6.2: Transfer impedance of steel foil armored cable (brand A, upper curve) compared to a conventional wire armored ground cable with embedded copper strand as protective earth litz (brand B, lower curve)
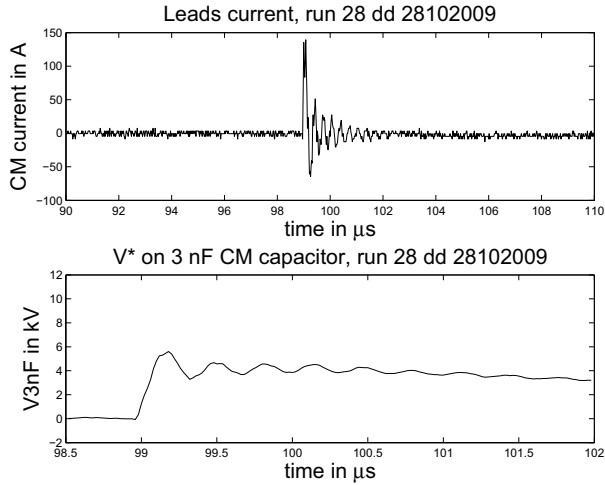
Figure 6.3: Injected CM current (top) and calculated voltage over the CM capacitor (bottom). Pleas note the different time scales on the x-axis in both figures.

6.1.3 Power input circuit

The input filter for the power is sketched in the inset of Fig. 6.1. The CM filter consists of two coupled coils and a 3 nF, 3 kV capacitor C_{CM} connecting the electronic null to the metallic lamp housing. The current to charge and discharge the lamp in case of lightning has to flow through C_{CM} and the leads to the gas-discharge luminair. If the pole would have been metallic, this current would have flown in the pole which for safety reasons would have been connected to the horizontal ground wire and local ground electrode. For the DC part of the current, only a path via leakage resistances was available. The stray inductance of the coils acts as differential mode filter together with capacitor C_{DM}. A single capacitor is shown, but several were present, also after the diode bridge. The large CM currents associated with lightning likely saturate the magnetic core of the coils, as do the injected currents in the tests.

Remarkably enough, the power input fuses of the driver were never damaged by lightning or in the tests. Always some parts of the electronics failed. Nevertheless, the TOP unit withstood the fast transient burst test up to 4.4 kV (100 kHz pulse repetition rate, bursts of 4 ms duration). The CM current in these tests amounted to 55 A, measured by a CM current probe.

The difference between the TOP and the CPO Xt electronic design is: better routing and better placement of MOV protection devices at the power input terminals, and local protection measures near active components. The selection was based on measured vulnerability with respect to CM currents.

6.2 Series of tests

The tests in the high-voltage laboratory were in order of increasing severity.

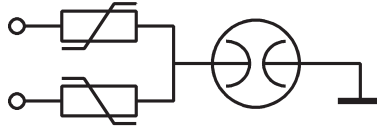- The discharge of a 0.5 μF high voltage capacitor over a 27 μH coil, where the

Figure 6.4: Design of the MOV-spark gap protection circuit

voltage was coupled to the lamp via a small capacitor of a few 100 pF up to 5 nF.

- Direct injection from the LSG.

- A chopped waveform of the LSG, where the lamp was part of the chopping spark gap.

With the capacitor discharge, the injection circuit is floating and it could be coupled directly to the lamp. With the LSG, the power was coupled via a 90 kV isolation transformer that ensured safety to the other lab equipment. The secondary was either floating or one lead was connected to ground (TT configuration). In all cases a powerline filter was installed at the feeding point. We enhanced the CM current capability of the filter with two 47 nF 10 kV capacitors between the power leads and local ground, mounted at the lamp side of the filter. As CM current probes we used the 8538 and 110 by Pearson, or a Fischer F75.

6.2.1   Capacitor discharge tests

Fig. 6.3 shows the CM current injected on the lamp with the capacitor discharge. The TOP driver survived this test. The voltage over C_{CM} has been calculated by integrating the current

$$V_{CM} = \frac{\int I_{CM} dt}{C_{CM}}. \tag{6.1}$$

For the test shown, the peak value of V_{CM} was less than 5 kV. The unit failed in a test with a larger current of up to 170 A, where the calculated voltage was approximately 10 kV. The capacitor is self-healing and it proved still to be intact after the second test. After removal of the potting, the damage to the electronics was confirmed to be identical the one caused by lightning in the actual installation. As a first remedy, we mounted a provisional overvoltage protection directly on the power terminals of the driver. The protection consisted of two varistors suited for 230 V power between the terminals and a 6 kV CM spark gap.

Even with the spark gap shorted, this protection did not suffice for the TOP. On the other hand, the CPO Xt driver survived this kind of test with currents up to 1 kA without the additional protection.

In order to partially remedy the lack of a conducting lamppost, we first installed a three lead cable with one lead as protective earth (PE) between the lamp and the power source. The CM current was shared equally by the three leads, so the PE did
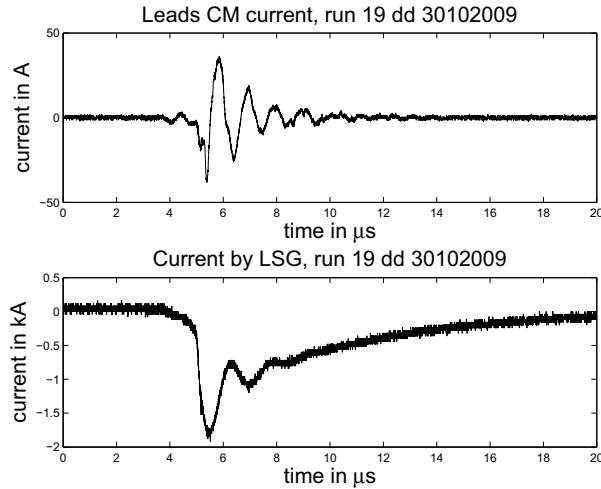
Figure 6.5: CM current in the leads (top) and current injected by the LSG (bottom) on the lamp.

not provide much protection at this current wave form (Fig. 6.3) with a dominant 3 MHz component. Next we included a 22 m section of the brand B cable mentioned in Section 6.1. The cable was wound on a reel to store the length. The armor was used as PE and shield, and was connected to the power ground and the lamp. With a 1.8 kA current in the armor, the CM current in the power leads remained smaller than 25 A and the TOP survived.

6.2.2 2MV lightning surge generator tests

The luminary with the TOP driver was connected via the armored cable again, and connected to the LSG. A number of tests were carried out. We present data with the most intense interference, obtained with a generator setting of 1 MV and coupling the generator to the luminary via a 0.8 m long spark gap to increase the current steepness. Power arrived via the brand B cable, still on the reel. Fig. 6.5 displays the CM current through the leads, measured at the ground end and the injected current through the cable. The leads CM current was less than $1/25^{th}$ of the cable current. The voltage over the CM capacitor is calculated again assuming that all leads current arrived at the electronic driver. In case the distributed cable capacitance takes its current share, the voltage over the CM capacitor is reduced. The calculated CM voltage was smaller than 3 kV; accordingly the TOP driver survived. In the same setup the CPO Xt survived 4 kA with a twin lead cable, without any armor or shield. Next, the luminary was mounted in a 10 m tall composite lamppost placed next to the LSG, and a 1 meter large spark gap was kept between the top of the LSG and the lamppost. Because of the lower impedance of the now-straight armored cable, the current was much larger. The protection ratio provided by the armor is again large, a factor of 20 using the ratio of peak to peak values for the current through the leads and the LSG current. Flashing over of the 1 meter spark gap easily led to damage of

the TOP driver, although it survived one or two strokes of about 2.5 kA. In all later measurements on the TOP, we connected the LSG directly to the lamp.

We also investigated the influence of the brand A power cable. The cable in the lamppost remained the armored cable as before, but shortened to about 13 m. A provisional connection point was made at the foot of the lampposts, where we measured the injection current through the armored cable into the lamppost and the CM current of both leads. The isolation transformer provided the power via two 22 m long brand A cables in parallel for phase and neutral. We compared a balanced 230 V power circuit and a circuit with one terminal grounded at the transformer (TT configuration).

At the mounting point all armors are connected together and connected to the ground connection at the transformer. Variable impedance between mounting point and transformer ground simulated the actual grounding impedance at the lamppost, estimated to be approximately 100 Ω.

With the balanced power circuit, the brand A decreased the protection ratio to a factor of 8. In the TT configuration this was further reduced to a factor of 4. Both effects are attributed to the high Z_t. Again, a local protection by two MOVs and a spark gap at the base of the lamppost proved to be ineffective.

6.3   Discussion

The tests mentioned above proved that the TOP drivers can be damaged by CM currents. Question is how currents with similar effect can be caused by lightning. There are several possibilities:

1. Upward leader formation without growth into the full discharge.

2. Induced currents due to the decaying electric field upon lightning at some distance.

3. Currents in the soil, entering the power systems through the Z_t of the ground cables.

Item 1: Currents between tens up to a kA should be considered [Mik05]. For the actual installation it is difficult to reconcile this with the large number of units that failed and with the visual inspection which revealed no damage. However, even smaller quasi-continuous currents may cause damage. In fact, any lightning phenomenon that brings more than 10 μC sufficiently fast to the luminary before it leaks away may overcharge C_{CM}. A ground wire was not effective at high frequency, as discussed in Section 6.2.1. But at low frequency, it provides a current path to the gas-discharge luminair in parallel with C_{CM} and acts as a minimal metal lamppost.

Item 2: Electric fields of several tens of kV/m exist under charged clouds. Consider the lamp as a $d = 0.8$ m diameter sphere, mounted at $h = 15$ m above the ground, exposed to a vertically polarized wave with an electric field of 5 kV/m ([Nuc90, Fig. 2a]). Such a field has been observed at 1 km distance from a stroke [Lin79]. The capacitance of the sphere C_s with respect to ground is approximately 45 pF. C_{CM} can be considered as the low-voltage arm of a divider with C_s exposed to 75 kV. The voltage over C_{CM} is then 1.1 kV. Because of the capacitive divider, the voltage over
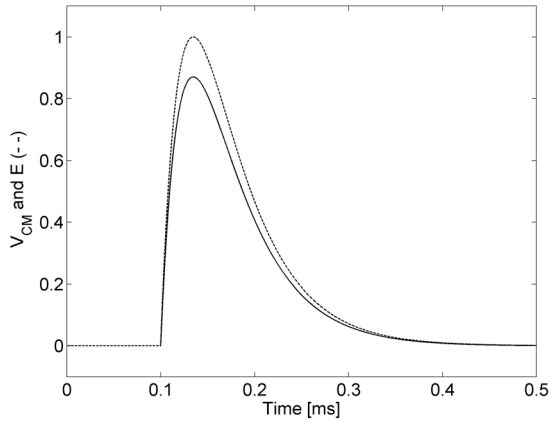
Figure 6.6: Calcutlaed V_{CM} in kV and assumed excitation field E in units of 5 kV, in a model with 25/50 μs rise fail time.

C_{CM} does not depend strongly on the exact time behavior of the lightning induced wave. We calculated the response to a 1 V/m vertically polarized plane wave at 1000 frequencies of 50 kHz up to 50 MHz [Fek10]. The luminair was modeled as an ellipse of 0.8 m $\times$ 0.3 m, connected via C_{CM} to a perfect ground via a 2 mm diameter wire, with a fixed resistance to ground at the bottom. Resonances occur on the wire at $h = \lambda/4 \times 1, 3, 5$, with λ the wavelength. We investigated a number of waveforms $E(t)$ in time domain to ascertain that the peak voltage over C_{CM} was related to the peak electric field. Rise times were chosen between 0.5 and 25 μs, decay times between 20 and 100 μs. The excitation waveform $E(t)$ was Fourier transformed into $E(f)$ over 10^5 points with 10 ns spacing. The FEKO frequency domain transfer $T(f)$ between the unit excitation field and the current through C_{CM}, $I_{CM}(f)$, was interpolated to cover the frequency range of the excitation waveform.

The time domain current $I(t)$ through C_{CM} was obtained from an inverse transform of $E(f) * T(f)$. The voltage followed from integrating $I(t) : V_{CM} = \int I(t')dt/C_{CM}$. Fig. 6.6 shows an example for an electric field of 25/50 μs rise/fall time. The current in the wire is proportional to frequency up to about 1 MHz. The capacitor integrates the current; as a result V_{CM} depends on the peak excitation and less on the wave shape. Table 6.1 specifies the peak current at the top and bottom of the wire inside the pole when excited by a 5 kV/m wave of 0.5/20 μs rise/fall time, for three values of the resistance towards the soil. The table also shows that the peak voltage is barely influenced by the resistance R_g at the base.

Item 3: The bare copper ground wire is in parallel with the power cable shields in the soil, and effectively diverts lightning induced soil current from those shields. Accidental continuous current in the luminair and its leads only can flow to earth at the feeding point in the TT configuration. A modification of the TT configuration into TNC would avoid this.

The system has been partly adapted now and a substantial number of poles has been equipped with a ground wire from the base to the TOP luminair. In a recent

lightning storm, all luminaires with ground wire remained functional whereas many without ground wire did not, as before. In view of our test results, LF phenomena, such as continuous currents should still be considered as a likely cause of damage.

6.4 Conclusions

The test revealed that the TOP electronic driver is quite susceptible to lightning induced CM currents. Two local remedies, a local overvoltage protection and improved cabling inside the poles, turned out to be insufficient. The influence of the high transfer impedance of the power cable in situ has been demonstrated by the measurements.

The main outcome of the investigations is that the total lightning safety strongly depends on installations details such as non-metallic poles, lack of ground wire, and power cables with large transfer impedance. These items are often beyond the control of the luminair manufacturer, who is then obliged to extremely harden his product. In the actual installation, a good choice is to replace the drivers by the CPO Xt. These units have a built-in protection as sketched in Fig. 6.4.

Table 6.1: Current I in A at the top and the bottom of the wire to the luminair for a 0.5/20 μs excitation of 5 kV/m, with resulting voltage over the C_{CM} in V, for different resistance top ground

R_g	0	10	50
	[Ω]	[Ω]	[Ω]
I_{top}	9.75	9.57	8.89
I_{bottom}	36.	35.4	32.9
V_{CM}	878.	875.	871.

Chapter 7

Two horizontal grounding electrodes

In this chapter, measurements and a model are described to derive the current distribution over a set of two horizontal grounding electrodes for frequencies between 50 Hz and 1 MHz. These kind of electrodes can be used as grounding for lightning protection.

7.1 Introduction

The lack of knowledge of the current distribution in a grounding electrode or wire is a classic problem in power delivery and lightning protection.

Computational problem has been extensively studied [Bri90, Bri95, Grc96, Ols96, AT04] and several experiments have been performed [Daw91, Ger99, Sek98, Buc05]. These experiments have been mostly in the power frequency range or performed with high-impulse currents resembling a lightning stroke. The current distribution over a set of two horizontal grounding electrodes near the Dommel, a local river, has been measured for frequencies between 50 Hz and 1 MHz. This range covers the power frequency at the low end, and most, if not all, frequencies important for lightning. These 50 mm^2 copper wires were 75 m long and were buried at the depth of 0.5 m, running in opposite directions; see Fig. 7.1. Several pits lined with 50 cm diameter plastic tubes allowed access to the wire at the positions indicated. The wire ran almost parallel to a 4 m wide shallow river at the distance of approximately 13 m. As a result the soil was quite humid, and the groundwater level was at this depth varying between 0.4 and 1 m, depending on rain fall. Nearby buried metal included, first, the safety grounding of the street lighting which was a bare 25 mm^2 copper wire, which ran parallel to the power cable and was assisted by vertical electrodes, and secondly the reinforcement of the 1.5 m diameter sewage pipe shown in Fig. 7.1.

7.2 Experimental set-up

In this experiment two setups were used, one at fixed position for the current injection, and a second mobile setup for measurement of the current and voltages at each pit.
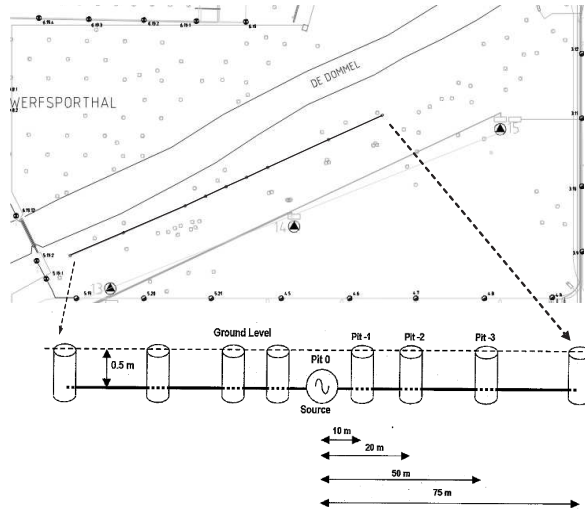
Figure 7.1: Actual measurement set-up and schematic view.

All electronic equipment in both setups was locally powered by two motor generators in order to avoid current leakage to other grounded terminals.

The two horizontal grounding wires were interrupted in pit 0, and the current I_{inj} was injected by two identical amplifiers (in Fig. 7.2 A1 and A2: AR AD40-1) driven by signals with opposite polarity. The maximum current was 1.6 A. The frequency range was DC up to 1 MHz. A current probe (P1: Pearson 110) measured the injected current I_{inj}. Two twisted leads delivered the voltage signals directly to the wire ends in the pit. Current and voltage signals were registered by a 4 channel digital oscilloscope (O: Tektronix TDS3054) with subsequent data transfer to a laptop computer. The signal from the P1 probe was used as a reference for amplitude and
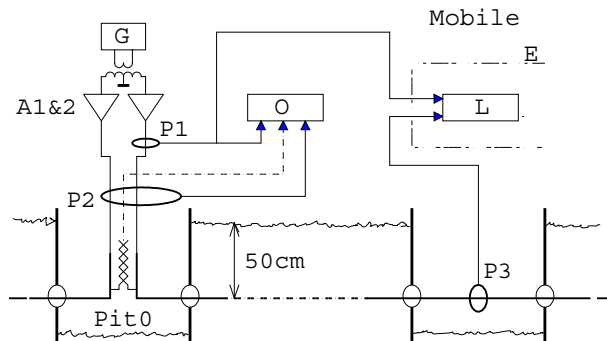
Figure 7.2: Schematic view of the setup at Pit 0 for injection and Pit n for measurement.
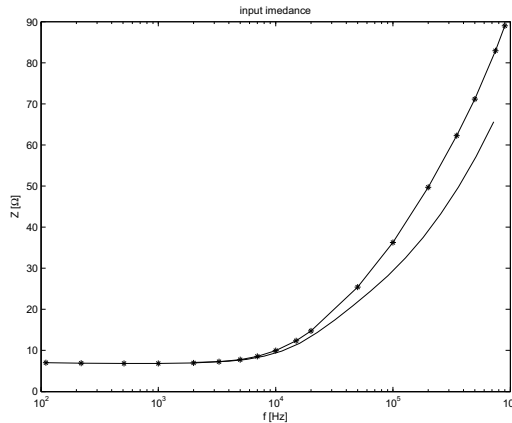
Figure 7.3: Measured input impedance '*-' and simulated input impedance '-' for 100 Hz to 1 MHz.

phase. The measured current and voltage provided the series input impedance Z_i of the wires. The unbalanced current in the wires due to leakage resistance and stray capacitances was measured as a check by P2 (another Pearson P110), and was always kept well below 1 % of the wire current by adjusting the gain of one amplifier. The wire current at the other pits was measured by a third current probe P3: a split core Pearson 3525 with insertion impedance smaller than 0.05 Ω. Its signal was recorded in amplitude and phase by a lock-in detector L: EG&G 5302 in the mobile setup. The reference signal for the lock-in was sent over a glass fiber optical link from the injection probe P1. The phase lag in the reference channel was determined. I_{inj} was determined by P1 and P3 simultaneously at the beginning and at the end of a measurement run. The amplitudes reproduced to within 1 %, the phase to within 5 degrees above 1 kHz. In order to avoid interference, all mobile equipment was placed in an EMC cabinet (E) in Fig. 7.2. Voltages were measured by probes via wires carefully positioned over the soil, with the EMC cabinet connected to the wire as a reference. Voltages at 2 and 5 m distance from the pit in the four directions were measured to determine the ground resistance.

7.3 Results

The input impedances of the horizontal wires are measured and simulated. One of the wires is called "West" and the other is called "East". In Fig.7.3, the measured and simulated input impedance results for frequencies from 100 Hz to 1 MHz are shown. The simulated and measured curves lie on the tops of each other, i.e. except for frequencies higher than 10 kHz, at which of material parameters of the ground had to be taken into account. For these high frequencies the simulated and measured curves show similar shapes, although they differ. The ground resistance can be determined from the simulated data. In this case the resistance is equal to 147.5 Ω.

The normalized current amplitude measured at the different pits is shown for the
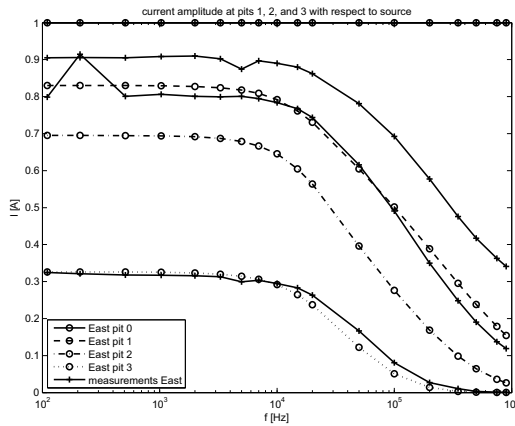
Figure 7.4: Measured current '+-' and simulated current'0-' for 100 Hz to 1 MHz for "East" wire.

"East" wire, in Fig. 7.4, and "West" wire in Fig. 7.5. The current amplitude for the wires is simulated and measured for the same frequencies as the input impedance, from 100 Hz up to 1 MHz. The simulated current amplitudes for the "East" and "West" wires show no difference in both figures. However, the measured current amplitudes for the two horizontal wires are different. In Fig. 7.4, the current of the "East" wire measured in pit 3 is higher than the current measured at pit 3 of the "West" wire, as is shown in Fig.7.5. Also, in Fig.7.4 a measurement error is shown in the data of the measured current at pit 2. All simulated data have lower current values than the measured ones, except the simulated data of the East wire at pit 3.
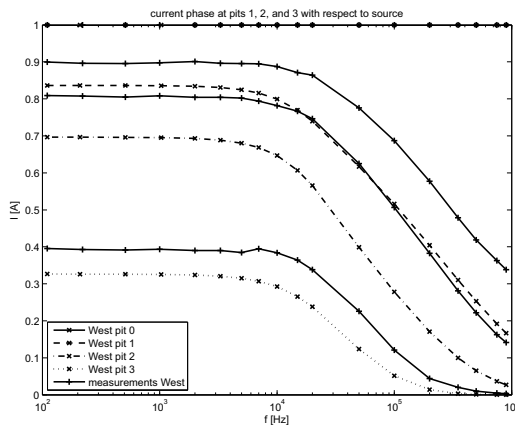

Figure 7.5: Measured current '+-' and simulated 'x-' current '*-' for 100 Hz to 1 MHz for "West" wire.

7.4 Discussion

The current distribution over a set of two horizontal grounding electrodes has been measured for frequencies between 50 Hz and 1 MHz. The overall trend of the results retrieved by simulation resemble quite well the results retrieved by measurements. First, a linear correlation is shown for low frequencies. Furthermore, based on the measurements, a high ground resistance at the start of the wire or an extra load at the end of the wire was expected. Secondly, the introduction of the wide shallow river as a metal conductor into the simulation showed no difference. However, this is expected to cause the difference between measurements and simulation. Because of the quite humid soil, the current probably spreads more into the ground. Lastly, the introduction of a layered ground into the simulations had no influence on the results.

7.5 Conclusion

The measurements at the horizontal grounding electrodes have been carefully performed. As a result, a reliable measurement of the current distribution over a set of two horizontal grounding electrodes has been conducted for power frequencies and most frequencies important for lightning. The simulation was improved by using the ground resistance, determined from the measurements. However, differences have been shown in the simulation details, which can be contributed to the many unknowns present in the ground. It can be concluded that caution is required for simulation models, which are used to determine the current distribution of horizontal grounding electrodes, because of the many unknowns.

Chapter 8

Conclusions and recommendations

8.1 Conclusions

The goal of the research was to define and validate a model for the disturbance current in buildings and installations, in particular disturbance currents caused by lightning. It should give insight into the errors and uncertainties of cable and wire implementation.

At the end of each chapter the relevant conclusions for the chapter have been given. Here general conclusions of the thesis are given.

- Current injection measurements can solve specific questions concerning the lightning protection. For instance wether the lightning protection is conducting like expected. In [IEC06, Part 1, annex D] only periodic visual inspections and tests of resistance to ground are recommended. The current injection measurements showed the possibility of existing un-intended conducting materials and are advisable for high risk buildings or structures and buildings with a high economical value.

- The reduced model of the new pharmaceutical plant correctly produces the measured current distribution between the roof grid and the steel skeleton. The copper roof grid connects the lightning capture rods and will be important when a lightning strike hits mid-roof. In all other cases the denser and heavier building skeleton appears to be a better protection against lightning. The last is also concluded from the two short one-day measurements.

- Total lightning safety strongly depends on installations details such as used cables and non-conducting parts. Armored and shielded cables used inside buildings show, because of lower Z_t, reduction in disturbance voltages in respect to unshielded cables.

- Additional interconnects to ground constructions cause a reduction of the lightning current inside a structure. They shift the resonance frequencies upwards and reduce the excitation of internal building resonances. Unrealistic artefacts in models should be avoided by including a sufficient number of interconnects.

8.2   Recommendations for future work

An overall recommendation for this work is that more buildings and especially installations should be investigated, to retrieve more information to implement into an industrial design code.

Another recommendation is to implement one complete connected earth structure throughout the whole building. As measurements showed the distribution current had a tendency to flow through the metal building instead of flowing trough the available down-conductors. This is in contradiction with the expectations given by the lightning protection zone principle.

8.2.1   Collaboration with industry

The project is part of the IOP EMVT programme, which provided two meetings a year with representatives of industry. This was to improve the collaboration with industrial partners. The first recommendation is to make the findings in this thesis available as add-ons to industrial design codes, which was one of the original goals of the research project. A first step would be to build an interface between the design software and the electromagnetic code to speed up the implementation, and to allow variations in the building design phase. In addition, faster EM computation using the 'marching-on' techniques would improve the usability of the developed methods.

8.2.2   Modeling

If more of the different installations was known and could be implemented into the model, also the calculations of the model could be improved. For instance in Chapter 3 the calculations where performed with only the Z-matrix of the construction. The calculations could be even more accurate when the Y-matrix of the construction was also implemented. This was not possible at the time of writing, because in FEKO the data of the charge density was not available in a way it could be processed. In the current version of FEKO this has changed, making the implementation of the Y-matrix possible. The expectation is that the voltages of the fieldbus and the 3-lead cable would increase a little. However, for the 2-lead cable with steel armor this increase could be higher. The process of translating S-parameter measurements of the cables into characteristic parameters should have a closer look as well. In particular in the situation of resonances. In the thesis of Steenstra [Ste08a] a recommendation was to implement the transmission line parameters into a model by having a standard set available in the design code. This recommendation can be adopted in this thesis as well. However, this only provides some first calculations with cables in a model, when comparing model results to measurement results there should always be looked at the actual cables used.

8.2.3   Measurement

Some improvements can be made by performing measurements as well. These recommendations are divided in the measuring of buildings and the measuring of cables.

Measuring of buildings

To start with the large measurement expeditions, it is recommended that although a one-day measurement can resolve specific questions concerning lightning protection, in order to investigate the current distribution in a building, more days are required. Especially, when the measurements are conducted on a Monday and the next measurements on a Friday, there is some time in between to interpret the results, which improves the total results of the expedition. It gives you time to measure for instance unexpected current paths.

Instead of two grounding electrodes it would be advisable to have at least four grounding electrodes in opposite directions. This could resolve the problem of the increased return current near the injection wires, because if the wires are evenly distributed the return current would show an evenly distributed behavior. However, this improvement could be problematic when the building is situated at only a few meters distance from a street or from another building.

Also it is preferable, to perform measurements with a gradually increased injection current to a maximum of 1.5 kA. However, this requirement would impose some persuading of the owners of the building or systems in the building, who express their concerns.

Measuring cable parameters

To retrieve the transmission line characteristic of the cable, measurements are performed with a triaxial measurement set-up. Two of these cable measurements in the frequency range of 10 Hz to 1 MHz are described in Chapter 2 and another in Chapter 6. The results of the measurements in Chapter 6 correspond with cable characteristics obtained with another commercial available measurement set-up used by Philip Lighting. The measurement equipment itself has a transfer characteristic as well. I would recommend to look into these characteristics, to verify that these do not influence the measurement as is assumed.

Appendix A

Implementation of Wu-King in the model in FEKO

The lightning channel used in the model is a 200-m-tall vertical current path. The upper path is a free-standing antenna on top of the source. In Chapter 3 we want to focus on problems which may occur, because the frequencies of lightning correspond with the resonance frequencies of the model structure. The paper written by T.T. Wu and R.W.P. King [Wu65], corrected in [She65], contains a formula (30), given in A.1, to calculate impedances, z^i in Ω/m to load an antenna to reduce resonances in this antenna, due to the length of the antenna. These impedances are needed to reduce the resonances due to the antenna, which is representing the lightning channel, and to put the focus on the resonances of the building, only.

$$z^i(z) = \frac{60\Psi}{h-|z|} \tag{A.1}$$

The h in this equation is the length of the antenna and the z is the position along the antenna. The factor Ψ is formulated as follows in A.2. This equation is constructed at the value where both the axial component of the vector potential and the total axial current have a maximum amplitude.

$$\Psi = 2[\sinh^{-1}(\tfrac{h}{a}) - C(2ka, 2kh) - jS(2ka, 2kh)] + \tfrac{j}{kh}(1 - e^{-2jkh}) \tag{A.2}$$

This equation (A.2) can be calculated with mathematical programs like Matlab and Mathematica. However the MOM code Feko [Fek10] has only some basic mathematical functions. This problem can be solved by approximating the given expressions.

$$\sinh^{-1}(\tfrac{h}{a}) = \ln\big(\tfrac{h}{a} + \sqrt{(\tfrac{h}{a})^2 + 1}\big) \tag{A.3}$$

and

$$\tfrac{j}{kh}(1 - e^{-2jkh}) = \tfrac{j}{kh} - \tfrac{j}{kh}\cos(2kh) - \tfrac{1}{kh}\sin(2kh) \tag{A.4}$$

The cosine integral is sometimes defined as

$$C(2kh) = \gamma + \ln 2kh - \int_0^{2kh} \frac{\cos(t)}{t} dt. \tag{A.5}$$

For large h the sine integral oscillates around $\frac{\pi}{2}$ and can be approximated.

$$S(2kh) \approx \frac{\pi}{2} + \frac{\sin(2kh)}{2kh} \tag{A.6}$$

The parameter Ψ is defined with these approximations as:

$$\begin{aligned} \Psi &= 2\ln\left(\frac{h}{a} + \sqrt{(\frac{h}{a})^2 + 1}\right) \\ &\quad - \frac{1}{kh}\sin(2kh) - 11.54 + 2\ln 2kh + \frac{j}{kh} \\ &\quad - \frac{j}{kh}\cos(2kh) - j\frac{\pi}{2} + j\frac{\sin(2kh)}{kh}. \end{aligned} \tag{A.7}$$

A.1 Wu-King implementation

The values for the Ψ is shown in Fig. A.1. This figure shows that the approximation is oscillating around the original calculation. When the approximations instead of the given formula for Ψ is used an error of approximately 6 % in amplitude and phase is introduced. This error is shown in Fig. A.2. The difference in the source current without and with the WuKing resistances profile is shown in Fig. A.3. This figure shows that the resonances due to the use of the antenna as a lightning channel are reduced.
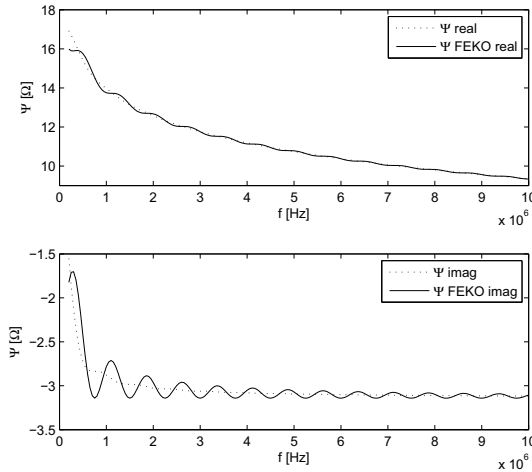
Figure A.1: Calculated Wu-King resistance Ψ in Ω for different frequencies and the approximation used in FEKO. The approximation is oscillating around the original. (top) real values for Ψ and the approximation (bottom) imaginair values.
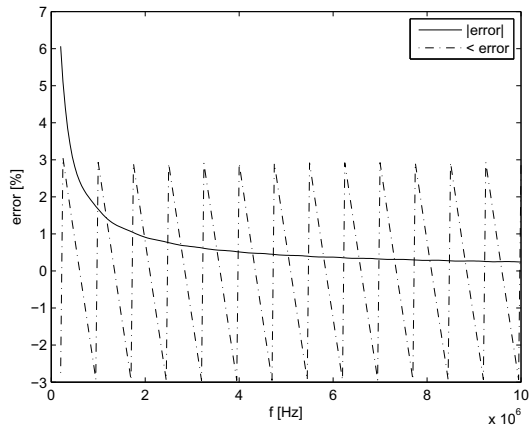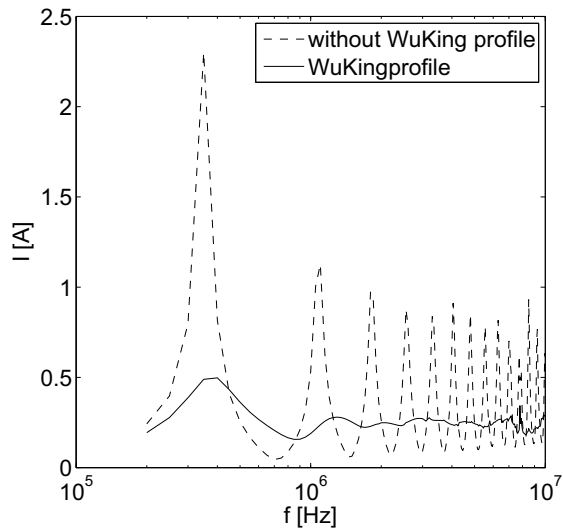
Figure A.2: Error between calculated Ψ and the approximated Ψ

Figure A.3: Source current without WuKing profile resistance and source current with WuKing profile resistances

Transfer parameters

B.1 Transmission line network

The general solution for a line voltage or current is given by the sum of two traveling waves along the line (Fig. B.1).

$$
\begin{aligned}
V_1(z) &= V_0^+ e^{-\gamma z} + V_0^- e^{\gamma z} \\
I_1(z) &= I_0^+ e^{-\gamma z} - I_0^- e^{\gamma z} \\
V_2(z+l) &= V_0^+ e^{-\gamma(z+l)} + V_0^- e^{\gamma(z+l)} \\
I_2(z+l) &= I_0^+ e^{-\gamma(z+l)} - I_0^- e^{\gamma(Z+l)}
\end{aligned}
$$

$$(B.1)$$

Expression for the S-parameters are given:

$$
V^- = S V^+
$$
$$
S_{ij} = \frac{V_i^-}{V_j^+}\Big|_{V_k^+ = 0} \quad \texttt{for} \quad k \neq j.
$$
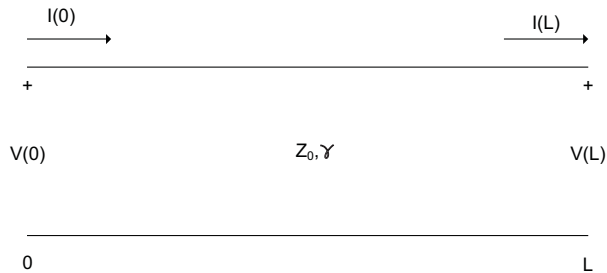
Figure B.1: Definition of the parameters of a two-conductor line in the frequency domain.

Expressions used to define a general impedance matrix are shown in the following equations:

$$V_1 = Z_{11}I_1 + Z_{12}I_2$$
$$V_2 = Z_{21}I_1 + Z_{22}I_2$$

$$Z_{11} = \left.\frac{V_1}{I_1}\right|_{I_2=0} = \frac{Z}{\tanh(\gamma l)}$$
$$Z_{12} = \left.\frac{V_1}{I_2}\right|_{I_1=0} = \frac{Z}{\sinh(\gamma l)}$$
$$Z_{21} = \left.\frac{V_2}{I_1}\right|_{I_2=0} = \frac{Z}{\sinh(\gamma l)}$$
$$Z_{22} = \left.\frac{V_2}{I_2}\right|_{I_1=0} = \frac{Z}{\tanh(\gamma l)}.$$

When the impedance matrix is used in combination with S-parameters the following equations express the conversion.

$$S11 = \frac{(Z_{11}-Z_0)(Z_{22}-Z_0)-Z_{12}Z_{21}}{(Z_{11}-Z_0)(Z_{22}-Z_0)-Z_{12}Z_{21}}$$

$$S12 = \frac{2Z_{12}}{(Z_{11}-Z_0)(Z_{22}-Z_0)-Z_{12}Z_{21}}$$

$$Z_{11} = Z_{22} = \frac{Z}{\tanh(\gamma l)}$$

$$Z_{12} = Z_{21} = \frac{Z}{\sinh(\gamma l)}$$

$$\bar{Z} = \frac{Z}{Z_0}$$

$$S11 = \frac{(\bar{Z}^2-1)\sinh(\gamma l)}{2\bar{Z}\cosh(\gamma l)+(\bar{Z}^2+1)\sinh(\gamma l)} \tag{B.2}$$

$$S12 = \frac{2\bar{Z}}{2\bar{Z}\cosh(\gamma l)+(\bar{Z}^2+1)\sinh(\gamma l)} \tag{B.3}$$

$$S21 = S12$$

$$S22 = S11$$

In Equations B.2 and B.3 Z_0 is the characteristic impedance of the measurement equipment and Z is the characteristic impedance of the line.

The Equations B.2 and B.3 can be used to determine the characteristic impedance parameter Z_c and propagation constant γ when the S-parameters are known. Two ways to calculate γ are shown.

$$\cosh(\gamma L) = \frac{1+S_{12}^2-S_{11}^2}{2S_{12}} \tag{B.4}$$

$$e^{-\gamma L} = \frac{1+S_{12}^2-S_{11}^2\pm\sqrt{1+S_{12}^4+S_{11}^4-2S_{11}^2S_{12}^2-2S_{12}^2}}{2S_{12}} \tag{B.5}$$

The calculation of γ should be looked at carefully because of problems which may occur in the phase information of the S-parameters, due to the length of the cable. Z_c can be determined by substituting γ.

$$\bar{Z} = \frac{S_{12}\cosh(\gamma L)-S_{11}-1}{S_{12}\cosh(\gamma L)+S_{11}-1} \tag{B.6}$$

$$\bar{Z} = \frac{Z_c}{Z_0}$$

$$Z_0 = 50\Omega \tag{B.7}$$

Equations B.4, B.5 and B.6 are also used in [Ste08a] and [Nij10].

The obtained parameters of Z_c and γ are needed to determine the line voltages and currents. Different ways to perform these calculations are shown in section B.2.

The characteristic impedance and propagation constant can be converted into the cable parameters by using the following expressions:

$$
\begin{aligned}
Z_c &= \sqrt{\frac{Z}{Y}} \\
\gamma &= \sqrt{ZY}.
\end{aligned}
$$

In these equations Z is the per unit length impedance of the cable and Y the per unit length admittance.

They can also be obtained in the following way:

$$
\begin{aligned}
(Z) &= (R) + j\omega(M) \\
(Y) &= (G) + j\omega(C).
\end{aligned}
$$

The coupling between the two loops is obtained by implementing the transformations used in [Dem00].

B.2 Determination of line voltages and currents

In this section the voltages and currents at the beginning and end of a cable are determined. In [Van78, Ch. 3] the line voltage and current are given as follows:

$$
\begin{aligned}
\frac{dV(z)}{dz} &= E_z - IZ \\
\frac{dI(z)}{dz} &= -VY \\
I(z) &= I_0^+ e^{-\gamma z} + I_0^- e^{\gamma z} \\
V(z) &= Z_0(I_0^+ e^{-\gamma z} - I_0^- e^{\gamma z}).
\end{aligned}
$$

In this equation I_0 is defined as:

$$
\begin{aligned}
I_0^+ &= = [K_1 + P(z)] \\
I_0^- &= = [K_2 + Q(z)].
\end{aligned}
$$

And $K_1, K_2, P(z)$ and $Q(z)$ are given as:

$$
\begin{aligned}
K_1 &= \rho_1 e^{\gamma z_1} \frac{\rho_2 P(z_2) e^{-\gamma z_1} - Q(z_1) e^{\gamma z_2}}{e^{\gamma(z_2 - z_1)} - \rho_1 \rho_2 e^{-\gamma(z_2 - z_1)}} \\
K_2 &= \rho_2 e^{-\gamma z_2} \frac{\rho_1 Q(z_1) e^{-\gamma z_1} - P(z_2) e^{-\gamma z_1}}{e^{\gamma(z_2 - z_1)} - \rho_1 \rho_2 e^{-\gamma(z_2 - z_1)}} \\
P(Z) &= \frac{1}{2Z_0} \int_{z_1}^{z} e^{\gamma v} E_z(v) dv \\
Q(Z) &= \frac{1}{2Z_0} \int_{z}^{z_2} e^{-\gamma v} E_z(v) dv
\end{aligned}
$$

Herewith:

$$\begin{array}{rcl} z_2 & > & z_1 \\ \rho_1 & = & \frac{Z_1 - Z_0}{Z_1 + Z_0} \\ \rho_2 & = & \frac{Z_2 - Z_0}{Z_2 + Z_0} \end{array}$$

When $z_1 = 0$ and $z_2 = L$ the above equations can be transformed as in [Van78, Ch. 5].

$$\begin{array}{l} I_m(0) = (1 - \rho_1) \frac{Q(0)e^{\gamma L} - \rho_2 P(L)e^{-\gamma L}}{e^{\gamma L} - \rho_1 \rho_2 e^{-\gamma L}} \\ I_m(L) = (1 - \rho_2) \frac{P(L) - \rho_1 Q(0)}{e^{\gamma L} - \rho_1 \rho_2 e^{-\gamma L}} \\ V_m(0) = -I_m(0)Z_1 \\ V_m(L) = I_m(L)Z_2 \end{array}$$

In [Tes97, Ch. 6] the voltage and current equations are given as follows:

$$\begin{array}{rcl} \frac{dV(z)}{dz} & = & -IZ \\ \frac{dI(z)}{dz} & = & -VY \\ V(z) & = & V_0^+ e^{-\gamma z} + V_0^- e^{\gamma z} \\ I(z) & = & Y_c(V_0^+ e^{-\gamma z} - V_0^- e^{\gamma z}). \end{array}$$

which results for $z = 0$ and $z = L$ in:

$$\begin{array}{l} I_m(0) = Y_c(1 - \rho_1) \frac{e^{\gamma L} - \rho_2 e^{-\gamma L}}{e^{\gamma L} - \rho_1 \rho_2 e^{-\gamma L}} \\ I_m(L) = Y_c(1 - \rho_2) \frac{1 - \rho_1}{e^{\gamma L} - \rho_1 \rho_2 e^{-\gamma L}} \\ V_m(0) = (1 + \rho_1) \frac{e^{\gamma L} - \rho_2 e^{-\gamma L}}{e^{\gamma L} - \rho_1 \rho_2 e^{-\gamma L}} \\ V_m(L) = (1 + \rho_2) \frac{1 - \rho_1}{e^{\gamma L} - \rho_1 \rho_2 e^{-\gamma L}}. \end{array}$$

These equation written in a compact matrix form are also known as BLT equation [Tes97].

$$\left(\begin{array}{c} V(0) \\ V(L) \end{array} \right) = \left(\begin{array}{cc} 1 + \rho_1 & 0 \\ 0 & 1 + \rho_2 \end{array} \right) \left(\begin{array}{cc} -\rho_1 & e^{\gamma L} \\ e^{\gamma L} & -\rho_2 \end{array} \right)^{-1} \left(\begin{array}{c} V_0^+ \\ V_0^- \end{array} \right) \tag{B.8}$$

$$\left(\begin{array}{c} I(0) \\ I(L) \end{array} \right) = \frac{1}{Z_c} \left(\begin{array}{cc} 1 - \rho_1 & 0 \\ 0 & 1 - \rho_2 \end{array} \right) \left(\begin{array}{cc} -\rho_1 & e^{\gamma L} \\ e^{\gamma L} & -\rho_2 \end{array} \right)^{-} 1 \left(\begin{array}{c} V_0^+ \\ V_0^- \end{array} \right) \tag{B.9}$$

This corresponds with the equations in [Pau08, Ch. 6].

To obtain natural propagation modes for multi conductor transmission lines a matrix representation is used.

$$\begin{array}{rcl} \frac{d(V(z))}{dz} & = & -(Z)(I(z)) \\ \frac{d(I(z))}{dz} & = & -(Y)(V(z)) \\ \frac{d^2(V(z))}{dz^2} & = & (Z)(Y)(V(z)) = -(\gamma)^2(V(z)) \\ \frac{d^2(I(z))}{dz^2} & = & (Z)(Y)(I(z)) = -(\gamma)^2(I(z)) \end{array}$$

The characteristic impedance and admittance matrix are evaluated:

$$(Z_c) = (S_v)(\Gamma)^{-1}(S_v)^{-1}(Z)$$
$$(Y_c) = (S_v)^{-1}(\Gamma)(S_v)(Z).$$

The fact that $[\gamma]^2$ is a diagonal matrix permits simple solutions.

$$
\begin{aligned}
(E(z)) &= \begin{pmatrix} e^{-\gamma z} & 0 \\ 0 & e^{-\gamma z} \end{pmatrix} \\
(V(0)) &= (S_v)\{(a) + (E(L))(b)\} \\
(V(L)) &= (S_v)\{(E(L))(a) + (b)\} \\
(I(0)) &= (Y_c)(S_v)\{(a) - (E(L))(b)\} \\
(I(L)) &= (Y_c)(S_v)\{(E(L))(a) - (b)\}
\end{aligned}
$$

In these equations a and b are Greens functions. These expressions correspond with the equations used in [Djo87].

B.3 Measurement set-up transmission line parameters

The S-parameters are retrieved by measurements. The measurement set-up consists of the inner conductors and the armor or shield of the cable, also known as the differential mode loop (DM). The other is the armor or shield with the L-shaped bar, also known as the common mode (CM) loop. In this thesis two ways are used to accomplish this. The first and most used in this thesis is shown in Fig. B.2. In this measurement set-up a cable is pressed into a corner of a L-shaped bar. The conductors of the cable are represented as one connection and are connected to the connector pin. These connectors are attached to metal cases at both sides of the L-shaped bar. The armor or shield, possibly with an additional copper litz, are represented as one connection and are connected to the metal casing at both sides. The metal casing at both sides is connected by a wire with connector pins. These connectors are attached to the L-shaped bar.

B.3.1 Measurement equipment

For the frequency range of 300 kHz to 1.8 GHz the spectrum analyzer HP 9643 A (100 kHz -1.8 GHz) and a S-parameter set, HP 85046A (300 kHz - 3 GHz) are used as the source generator and also as voltage meter. This combination sends a signal of 0 dBm through the cable and determines the S-parameters according to the transmission line principle. To retrieve the S-parameters of the DM loop the generator and voltage meter are connected to the connectors on top of the metal casings, which are attached to the inner conductors of the cable at both sides. The other connectors are terminated with a resistance of 50 Ω [Ste08a]. To retrieve de S-parameters of the CM loop the generator and voltage meter are connected to the connectors at the L-shaped bar or copper tube and the other connectors are terminated with a resistance of 50 Ω.
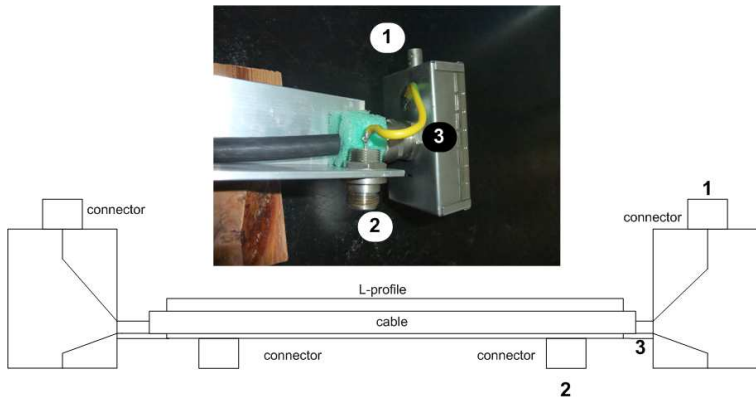
Figure B.2: The transmission line measurement set-up. (Top) Picture of the set-up. (Bottom) Schematic overview. The numbers in the picture correspond with the numbers in the schematic overview. The cable is pressed into the corner of the L-shaped bar. The inner conductors are represented as one connection and connected to the pin of the connectors on top of the metal casings at both sides. The shield or armor is represented as a connection connected to the metal casing. The metal casing is connected by a wire to the pins of the connectors attached to the L-shaped bar.

Lightning parameters

The lightning parameters are given in [IEC06, Part 1, Annex B] and also shown Table C.1. In this table the roman numbers indicate the lightning protection level. k is the correction factor for the peak current. The T_1 is the rise time and T_2 the decay time. The corresponding front and tail time constants are τ_1 and τ_2 respectively. For each lightning protection level a maximum of minimum set of lightning current parameters is fixed. The maximum values of lightning current parameters relevant to lightning protection level I will not be exceeded, with a probability of 99 %. The maximum values of the parameters are used to design lightning protection components. The minimum values of the parameters are used to derive the rolling sphere radius in order to define the lightning protection zone, which cannot be reached by direct strike. The approximating expression for the lightning current i reads [IEC06]

$$i(t) = \frac{I}{k} \times \frac{(t/\tau_1)^{10}}{1 + (t/\tau_1)^{10}} \exp(-t/\tau_2). \tag{C.1}$$

In Fig. C.1 the lightning current for lightning protection level I first stroke is shown with T_1 and T_2 indicated.

Table C.1: Model parameters of first and subsequent lightning stroke, after [IEC06]

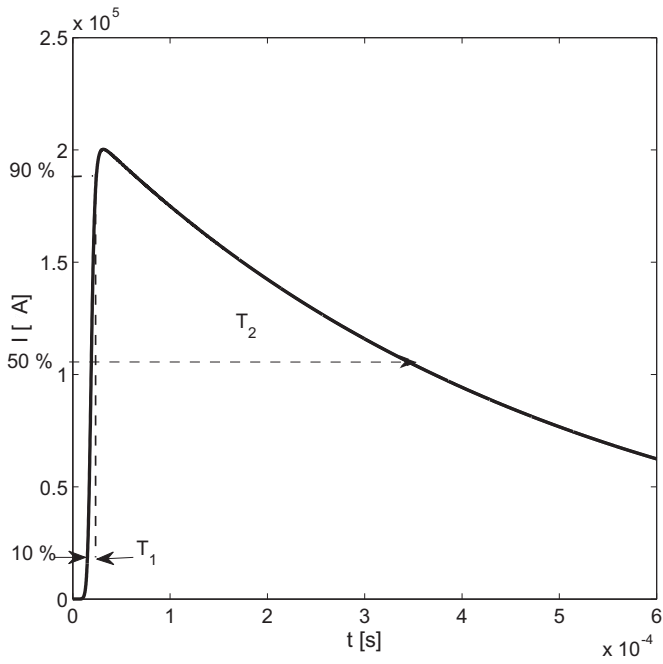| Parameter	first			subsequent		
	I	II	III-IV	I	II	III-IV
I [kA]	200	150	100	50	37.5	25
k		0.93			0.993	
τ_1 [μs]		19			0.454	
τ_2 [μs]		485			143	
T_1/T_2 [μs/μs]		10/350			0.25/100	

Figure C.1: Lightning current for lightning protection level I first stroke with with T_1 and T_2 indicated

List of abbreviations

APEMC	Asian Pacific EMC
BLT-method	Baum-Liu-Tesche-method
CM	Common Mode
CPO Xt	drivers called 'Cosmopolis Extreme'
DC	Direct Current
DM	Differential Mode
EEC	European Economic Community
EM	Electromagnetic
EMC	Electromagnetic Compatibility
EMI	Electromagnetic Interference
EMVT	Electromagnetische Vermogenstechniek
EPC	Earthed Parallel Conductor
FFT	Fast Fourier Transform
HV	High Voltage
ICLP	International Conference on Lightning Protection
IEC	International Electrotechnical Commission
IFFT	Inverse Fast Fourier Transformation
ILP	Internal Lightning Protection
IOP-EMVT	Innovatief Onderzoeksprogramma Electromagnetische Vermogenstechn
LF	Lightning Frequency
LP	Lightning Protection
LSG	Lightning Surge Generator
MoM	Method of Moments
MOV	Metal Oxide Varistor
PC	Personal Computer
PE	Protective Earth
PEC	Perfect Electric Conductor
RF	Radio Frequency
SIPDA	Siposio International de Protecao Contra Descargas Atmosfericas
TL	Transmission Line
TOP	Typical Outdoor Product
UTP	Unshielded Twisted Pair

Bibliography

[Ala02] G. Ala and M. Di Silvestre. "A simulation model for electromagnetic transients in lightning protection systems". *IEEE Trans. Electromagn. Compat.*, vol. 44, no. 4 pp. 539–554, 2002.

[And09] G. Andrieu, A. Reinex, X. Bunlon, J. Permantier, L. Koné and B. Démoulin. "Extension of the "Equivalent Cable Bundle Method" for modeling electromagnetic emissions of complex cable bundles". *IEEE Trans. Electromagn. Compat.*, vol. 51 pp. 108–118, 2009.

[AT04] V. Arnautovski-Toseva and L. Grcev. "Electromagnetic analysis of horizontal wire in two-layered soil". *Journal of Computational and Applied Mathematics*, vol. 168 pp. 21 – 29, 2004.

[Bab08a] Y. Baba and V. Rakov. "Applications of electromagnetic models of the lightning return stroke". *IEEE Trans. Power Delivery*, vol. 23 pp. 800–811, 2008.

[Bab08b] Y. Baba and V. Rakov. "Electric and magenetic fields predicted by lightning return stroke electromagnetic models". In *20 th International Zurich Symposium on Electromagnetic Compatability*, pp. 117–120. Zurich, Zwitserland, 2008.

[Bar08] G. Bargboer, A. van Deursen, C. Nguyen, H. Steenstra, T. Bosveld, R. Parrado Curros and J. Broekmeulen. "Finding weak spots in lightning protection". In *Proceedings Int. Symp. on EMC (EMC Europe '08)*, pp. 269–274. Hamburg, Germany, 2008.

[Bar09] G. Bargboer and A. van Deursen. "Lightning protection of a pharmaceutical plant, measurements and modeling". In *Proceedings ICEAA 2009*, pp. 886–889. Torino, Italy, 2009.

[Bar10] G. Bargboer and A. van Deursen. "A case study of lightning protection, current injection measurement and model". *IEEE Trans. Electromagn. Compat.*, vol. 52 pp. 684–690, 2010.

[Bau78] C. Baum, T. Liù and F. Tesche. In *On the analysis of general muliconductor transmission-line networks*. Iteraction Notes, Note 350, 1978.

[Bau92] C. Baum. "From the electromagnetic pulse to high-power electromagnetics". *Proc. IEEE*, vol. 80, no. 6 pp. 789 – 817, 1992.

[Bri90] G. Bridges. "Interface effects on the propagation constant and fields of a bare conductor burried in a lossy halfspace". In *IEEE Antennas en Propagation Society Symposium 1990. AP-S. 'Merging Technologies for the 90's'. Digest. 7th-11th May 1990*, vol. 1, pp. 332–335. 1990.

[Bri95] G. Bridges. "Transient plane wave coupling to bare and insulated cables buried in a lossy half-space". *IEEE Trans. Electromagn. Compat.*, vol. 37, no. 1 pp. 62 – 70, 1995.

[Buc05] C. Buccella, M. Feliziani, G. Manzi and F. Maradei. "Prediction of voltage and current porpagation in twisted wire pairs (twps) by a circuit model". In *Int. Symp. on Electromagn. Compat.*, pp. 51–55. Chicago, United States of America, 2005.

[Daw91] F. Dawalibi and N. Barbeito. "Measurements and computations of the performance of groundig systems buried in multilayer soils". *IEEE Trans. Power Delivery*, vol. 6, no. 4 pp. 1483 – 1490, 1991.

[Dem87] B. Demoulin, S. Assad and P. Degauque. "Analysis of the behavious of a shielded two-wire line in a disturbing environment". In *Proc. 7th Int. Zurich Symposium on EMC*, p. paper 34F6. Zurich, 1987.

[Dem00] B. Demoulin and A. van Deursen. "Deux approches pour établir le lien entre la notion usuelle d'impédance de transfert et le formalisme des lignes couplées". In *10 èm Colloque International & Exposition sur la Compatibilitè Electromagnètique (CEM2000)*, pp. 98–103. Clermont-Ferrand, 2000.

[Deu89] A. van Deursen, J. Wetzer and P. van der Laan. "Local protection of equipment in high voltage substations". In *6th Int. Symp. on High Voltage Engineering*, p. paper 31.03. New Orleans, LA, 1989.

[Deu93] A. van Deursen. *IEC 61000-5-2: Electromagnetic Compatibility, Part 5: Installations and Mitigation Guidelines; Section 2: Earthing and Cabling, EUT Report 93-E-275*. Eindhoven University of Technology, Eindhoven, The Netherlands, 1993.

[Deu01a] A. van Deursen, F. van Horck, M. van Helvoort and P. van der Laan. "Transfer impedance of non-magnetic conduits of various shapes". *IEEE Trans. Electromagn. Compat.*, vol. 43, no. 1 pp. 18–28, 2001.

[Deu01b] A. van Deursen, F. van Horck and J. van der Merwe. "A self-optimizing discretization scheme for 2d boundary element calculations". *J. of Electromagnetic Waves and Applications*, vol. 15, no. 4 pp. 461 – 476, 2001.

[Deu06] A. van Deursen, H. Smulders and R. de Graaff. "Differentiating/integrating measurement setup applied to railway environment". *IEEE Trans. Instrum. and Meas.*, vol. 55, no. 1 pp. 316–326, 2006.

[Deu09] A. van Deursen and V. Stelmashuk. "Sensors for in-flight lightning detection on passenger aircrafts". In *Proc. ESA Workshop on Aerospace EMC.* Florence, Italy, 2009.

[Deu10] A. van Deursen, G. Bargboer, M. Casanova and H. Misdom. "Lightning test on a electronic lamb driver". In *Proceedings of 9th international symposium on EMC*, pp. 575–578. Wroclaw, Poland, 2010.

[Deu11] A. van Deursen and G. Bargboer. "A case study on lightning protection, building resonances considered", 2011. Unpublished.

[Die85a] G. Diendorfer, W. Hadrian and R. Jobst. "Simulation von direkten Bliteinslägen in den Funkmast van Hochspannungsschaltanlagen, praktische durchfürung der Messungen". In *18th Int. Conf. on Lightning Protecton, ICLP*, pp. 171–174. München, Germany, 1985.

[Die85b] G. Diendorfer, W. Hadrian and J. R. "Simulation von direkten Blitzeinslägen in den Funkmast van Hochspannungsschaltanlagen, Möglichtkeiten und Grenzen der simulation". In *18th Int. Conf. on Lightning Protecton, ICLP*, pp. 165–170. München, Germany, 1985.

[Dij07] N. van Dijk. *New concepts for EMC standards applicalbe to multimedia products.* Ph.D. Thesis, Eindhoven University of Technology, Eindhoven, 2007.

[Djo87] A. R. Djordjeviċ and T. K. Sarkar. "Analysis of time response of lossy multiconductor transmission line networks". *IEEE Trans. Microw. Theory Tech.*, vol. MTT-35, no. 10 pp. 898 – 908, 1987.

[EMV11] IOP-EMVT. "[on-line] http://www.senternovem.nl/iopemvt/", 2011.

[Fek08] FEKO. *FEKO Users manual.* Stellenbosch, South Afrika, 2008.

[Fek10] FEKO. "[on-line] http://www.feko.info/", 2010.

[Ger99] A. Geri. "Behaviour of grounding systems excited by high impulse currents: the model and its validation". *IEEE Trans. Power Delivery*, vol. 14, no. 3 pp. 1008 – 1017, 1999.

[Grc96] L. Grcev. "Computer analysis of transient voltages in large grounding systems". *IEEE Trans. Power Delevery*, vol. 11, no. 2 pp. 815 – 823, 1996.

[Hei85] F. Heidler. "Analytische Blitzstromfunktion zur LEMP-berechnung". In *18th Int. Conf. on Lightning Protecton, ICLP*, pp. 63–66. München, Germany, 1985.

[Hel95a] M. van Helvoort. *Grounding structures for the EMC-protection of cabling and wiring.* Ph.D. Thesis, Eindhoven University of Technology, Eindhoven, 1995.

[Hel95b] M. van Helvoort, A. van Deursen and P. van der Laan. "The transfer impedance of cables with a nearby return conductor and noncentral inner conductor". *IEEE Trans. Electromagn. Compat.*, vol. 37, no. 2 pp. 301–306, 1995.

[Hen93] J. Hendry. "Panning for Lightning (including Comments on the Photos by M. Uman)". In *Wheaterwise*, vol. 45, no. 6 pp. 19, 1993.

[Hor98] F. van Horck. *Electromangetic compatibility and printed circuit boards*. Ph.D. Thesis, Eindhoven University of Technology, Eindhoven, 1998.

[Hou90] M. van Houten. *Electromagnetic compatibility in high-voltage engineering*. Ph.D. Thesis, Eindhoven University of Technology, Eindhoven, 1990.

[IEC97] IEC61000-5-2. *IEC61000-5-2: Electromagnetic Compatibility, Part 5: Installations and Mitigation Guidelines; Section 2: Earthing and Cabling*. IEC, Geneva, 1997.

[IEC06] IEC62305. *IEC62305: Protection against lightning*. IEC, Geneva, 2006.

[Ker07] A. Kern, F. Heidler, S. Seevers and W. Zischank. "Magnetic fields and induced voltages in case of a direct strike — comparison of results obtained from measurements at a scaled building to those of IEC 62305-4". *J. Electrostatics*, vol. 65 pp. 379–385, 2007.

[Laa98] P. van der Laan and A. van Deursen. "Reliable protection of electronics against lightning: Some practical applications". *IEEE Trans. Electromag. Compat.*, vol. 40, no. 4 pp. 513–520, 1998.

[Lin79] Y. Lin, M. Uman and R. Strandler. "Characterization of lightning return stroke electric and magnetic fields from simultaneous two-station measurements". *J. Geophys. Res.*, vol. 85 pp. 6307–6314, 1979.

[Mar02] R. Markowska, A. Sowa and L. Augustyniak. "Lightning effects in base stations of global systems for mobile communication". In *Int. Carpathian Conference on EMC (ICC'02) - Protection of Computer Systems against Electromagnetic Disturbances*, p. paper II.12. Rzeszow - Lancut, Poland, 2002.

[Met06] I. Metwally, F. Heidler and W. Zischank. "Magnetic fields and loop voltages inside reduced and full scale structures produced by direct lightning strikes". *IEEE Trans. Electromagn. Compat.*, vol. 48, no. 2 pp. 414–426, 2006.

[Mik05] M. Miki, V. Rakov, T. Shindo, G. Diendorfer, M. Mair, F. Heidler, W. Zischank, M. Uman, R. Thottappillil and D. Wang. "Initial stage lightning initiated from tall objects and in rocket-triggered lightning". *J. Geophys. Res.*, vol. 110 p. paper D02109, 2005.

[Miy08] S. Miyazaki and M. Ishii. "Role of steel frames of buildings for mitigation of lightning-induced magnetic fields". *IEEE Trans. Electromagn. Compat.*, vol. 50, no. 2 pp. 333 – 339, 2008.

[Mon98] E. Montandon and M. Rubinstein. "Some observations on the protection of buildings against the induced effects of lightning". *IEEE Trans. Electromag. Compat.*, vol. 40, no. 4 pp. 505 – 512, 1998.

[Nij09] J. Nijenhuis *Characterization and application of a reverberating chamber.* M.Sc. Thesis, Eindhoven University of Technology, Eindhoven, 2009.

[Nij10] J. Nijenhuis and A. van Deursen. "Interference coupling on armored installation cables, meaured in a reveberation chamber". In *Proceedings of APEMC Symposium 2010*, pp. 274–276. Beijing, Republic of China, 2010.

[Nuc90] C. Nucci, G. Diendorfer, M. Uman, F. Rachidi, M. Ianoz and C. Mazetti. "Lightning return stroke current models with specified channel-bas current: a review and comparison". *J. Geophys. Res.*, vol. 95 pp. 20395–20408, 1990.

[Ols96] R. Olsen and M. C. Willis. "A comparison of exact and quasi-static methods for evaluating grounding systems at high frequencies". *IEEE Trans. Power Delivery*, vol. 11, no. 2 pp. 1071 – 1081, 1996.

[Pau08] C. Paul. *Analysis of multiconductor transmission lines second edition.* John Wiley & Sons, Hoboken New Jersey, 2008.

[Pro10] Profibus. "[on-line] http://www.profibus.com/", 2010.

[Rak01] V. A. Rakov. "Transient response of a tall object to lightning". *IEEE Trans. Electromagn. Compat.*, vol. 43, no. 4 pp. 654 – 661, 2001.

[Rak03] V. Rakov and M. Uman. *Lightning: physics and effects.* Cambridge University Press, 2003.

[Sek98] S. Sekokia, H. Hayashida, T. Hara and A. Ametani. "Measurements of grounding resistance for impulse currents". In *IEE Proc. Gener. Transm. Distrib.*, vol. 145, pp. 693–699. 1998.

[She65] L. Shen and R. King. "The cylindrical antenna with nonreflecting resistive loading". *IEEE Trans. Antenna and Propagation.*, vol. 13, no. 6 p. 998, 1965.

[Ste08a] H. Steenstra. *Electro Magnetic Compatibility of Cabling and Wiring in Buildings and Installations.* Ph.D. Thesis, Delft University, Delft, 2008.

[Ste08b] H. Steenstra and A. van Deursen. "Reduction of conducted interference by steel armor in buried cables: Measurements and modeling". *IEEE Trans. Electromagn. Compat.*, vol. 50, no. 3 pp. 678 – 686, 2008.

[Tes97] F. Tesche, M. Ianoz and T. Karlsson. *EMC Analysis Methods and Computational Models.* John Wiley & Sons, New York, 1997.

[Uma94] M. Uman. "Natural lightning". *IEEE Trans. Industry App.*, vol. 30, no. 3 pp. 785 – 790, 1994.

[Van78] E. Vance. *Coupling to Shielded Cables.* John Wiley & Sons, New York, 1978.

[Wae03] J. van Waes. *Safety and EMC aspects of grounding, experimental studies in high-power systems.* Ph.D. Thesis, Eindhoven University of Technology, Eindhoven, 2003.

[Wu65]   T. Wu and R. King. "The cylindrical antenna with nonreflecting resistive loading". *IEEE Trans. Antenna and Propagation.*, vol. 13, no. 3 pp. 369–373, 1965.

[Zis06] W. Zischank, F. Heidler, J. Wiesinger, I. Metwally, A. Kern and M. Seevers. "Laboratory simulation of direct lightning strokes to a modeled building: measurements of magnetic fields and induced voltages". *J. Electrostatics*, vol. 60 pp. 223–232, 2006.

Acknowledgement/ Dankwoord

Curriculum Vitae

Geesje Bargboer was born on 16-02-1979 in Hellendoorn, The Netherlands.

After finishing the secondary school in 1996 she studied Electrical Engineering at Saxion University of Applied Sciences in Enschede, The Netherlands. After receiving the Bachelor of Science degree in telecommunication in 2001 she studied Electrical Engineering at Eindhoven University of Technology in Eindhoven, The Netherlands. In 2006 she graduated within the Electromagnetics group on uncertainties of radiated emission measurements in the near-field region.

From March 2006 she started a PhD project at Eindhoven University of Technology at Eindhoven, The Netherlands, financed by the Dutch Ministry of Economic Affairs of which the results are presented in this dissertation.